Nuclear IQGAP1 promotes gastric cancer cell growth by altering the splicing of a cell-cycle regulon in co-operation with hnRNPM

Andrada Birladeanu[1,5], Malgorzata Rogalska[2,5], Myrto Potiri[1,5], Vassiliki Papadaki[1], Margarita Andreadou[1], Dimitris Kontoyiannis[1,3], Zoi Erpapazoglou[1], Joe D. Lewis[4], Panagiota Kafasla[*,1]

[1]Institute for Fundamental Biomedical Research, B.S.R.C. "Alexander Fleming", 34 Fleming st., 16672 Vari, Athens, Greece

[2]Centre de Regulació Genòmica, The Barcelona Institute of Science and Technology and Universitat Pompeu Fabra, Dr. Aiguader 88, 08003, Barcelona, Spain

[3] Department of Biology, Aristotle University of Thessaloniki, Greece

[4]European Molecular Biology Laboratory, 69117 Heidelberg, Germany

[5]These authors contributed equally

[*]Correspondence: kafasla@fleming.gr

Summary

Heterogeneous nuclear ribonucleoproteins (hnRNPs) play crucial roles in alternative splicing, regulating the cell proteome. When they are miss-expressed, they contribute to human diseases. hnRNPs are nuclear proteins, but where they localize and what determines their tethering to nuclear assemblies in response to signals remain open questions. Here we report that IQGAP1, a cytosolic scaffold protein, localizes in the nucleus of gastric cancer cells acting as a tethering module for hnRNPM and other

spliceosome components. One of the consequences of the IQGAP1-hnRNPM interaction is to change the alternative splicing of the anaphase promoting complex (ANAPC), subunit 10 and is required for the hnRNPM response to heat-induced stress signals. Together, IQGAP1 and hnRNPM promote gastric cancer cell growth, and their genetic depletion leads to cell cycle arrest and halts tumour progression. We propose that in response to stress-signals IQGAP1 translocates in the nucleus to coordinate gastric tumour growth by recruiting spliceosome components that drive cell cycle progression.

Introduction

In humans, more than 95% of multi-exonic genes are potentially alternatively spliced (Pan et al., 2008; Wang and Burge, 2008). Precise modulation of Alternative Splicing (AS) is essential for shaping the proteome of any given cell and altered physiological conditions can change cellular function via AS reprogramming (Heyd and Lynch, 2011). The importance of accurate AS in health and disease, including cancer (El Marabti and Younis, 2018; Kahles et al., 2018; Oltean and Bates, 2013; Sveen et al., 2015), has been well documented. However, evidence connecting AS regulation to signalling comes mostly from few cases where localization, expression, or post-translational modifications of specific splicing factors such as Serine-Arginine-rich (SR) proteins or heterogeneous nuclear ribonucleoproteins (hnRNPs) (Heyd and Lynch, 2011; Shkreta and Chabot, 2015) are altered.

An abundant, mainly nuclear protein of the hnRNP family is hnRNPM, with four isoforms that arise from alternative splicing and/or post-translational modifications (Datar et al., 1993). The only nuclear role so far reported for hnRNPM is in spliceosome assembly and splicing itself (Kafasla et al., 2002; Llères et al., 2010),

including regulation of AS of other as well as its own pre-mRNAs (Hovhannisyan and Carstens, 2007; Huelga et al., 2012; Pervouchine et al., 2019). The association of hnRNPM with the spliceosome is abolished under heat-induced stress (Gattoni et al., 1996; Llères et al., 2010), suggesting its involvement in stress-related signalling pathways.

HnRNPM-regulated AS events have been linked to disease development and progression. Specifically, hnRNPM-mediated AS is deterministic for the metastatic potential of breast cancer cells, due to cell-type specific interactions with other splicing factors (Harvey et al., 2018; Hu et al., 2020, p. 8; Xu et al., 2014). Furthermore, in Ewing sarcoma cells, hnRNPM abundance and subnuclear localization change in response to a chemotherapeutic inhibitor of the PI3K/mTOR pathway, resulting in measurable AS changes (Passacantilli et al., 2017). Very recently, hnRNPM was shown to respond to pattern recognition receptor signalling, by modulating the AS outcome of an RNA-regulon of innate immune transcripts in macrophages (West et al., 2019).

Despite such growing evidence on the cross-talk between hnRNPM-dependent AS and cellular signalling, how distinct signals are transduced to hnRNPM and the splicing machinery remains unclear. Here, we present conclusive evidence of how this could be achieved. We describe a novel interaction between hnRNPM and the scaffold protein IQGAP1 (IQ Motif Containing GTPase Activating Protein 1) in the nucleus of gastric cancer cells. Cytoplasmic IQGAP1 acts as a signal integrator in a number of signalling pathways (Hedman et al., 2015; Smith et al., 2015), but there is no defined role for the nuclear pool of IQGAP1. With *IQGAP1* mRNA being overexpressed in many malignant cell types, the protein seems to regulate cancer growth and metastatic potential (Hu et al., 2019; Osman et al., 2013; White et al.,

2009). Moreover, aged mice lacking IQGAP1 develop gastric hyperplasia suggesting an important *in vivo* role for IQGAP1 in maintaining the gastric epithelium (Li et al., 2000). In the present study we show that this novel, nuclear interaction between hnRNPM and IQGAP1 links cellular signalling to hnRNPM-regulated AS in gastric cancer, a cancer type that has been associated with a significantly high incidence of AS changes (Kahles et al., 2018; Sveen et al., 2015). Additionally, we show that depletion of both interacting proteins results in tumour growth reduction, which makes them and their interaction interesting cancer drug targets.

Results

hnRNPM and IQGAP1 expression levels are significantly altered in gastric cancer.

Analysis of the hnRNPM and IQGAP1 protein levels by immunofluorescence on commercial tissue microarrays revealed increased hnRNPM and IQGAP1 staining in tumour as compared to normal tissue, especially in adenocarcinoma samples **(Figure 1A and Figure S1A-C).** This agrees with TCGA data analysis indicating significantly increased expression of both *IQGAP1* and *hnRNPM* mRNAs in stomach adenocarcinoma (STAD) vs normal tissue samples (**Figure 1B**). Furthermore, a strong correlation between the expression of the two mRNAs (*HNRNPM* and *IQGAP1*) in normal tissues (GTex) was revealed, which was reduced in normal adjacent tissues (Normal) and eliminated in STAD tumours (**Figure 1C**). Detection of hnRNPM and IQGAP1 protein levels in a number of gastric cancer cell lines by immunoblotting (**Figure 1D**) identified cell lines with similar levels of hnRNPM and low or high levels of IQGAP1 (MKN45, AGS and NUGC4, KATOIII), corroborating the TCGA data. Two of those STAD cell lines were used for further studies (NUGC4

and MKN45) since they have similar hnRNPM, but different IQGAP1 expression levels.

An interaction between hnRNPM and IQGAP1 was detected in nuclear extracts from both cell lines using immunoprecipitation with anti-IQGAP1 antibodies (**Figure 2A**). Treatment with RNaseA showed that the two proteins interact independently of the presence of RNA. This interaction also appeared DNA-independent (**Figure S2A and data not shown)**. Immunoprecipitation using anti-IQGAP1 antibodies from cytoplasmic extracts did not reveal interaction with the minor amounts of cytoplasmic hnRNPM (**Figure S2B and data not shown)**, indicating that if the proteins do interact in the cytoplasm, these complexes are less abundant compared to the nuclear ones.

There are previous reports of a small fraction of IQGAP1 entering the nucleus in a cell cycle-dependent manner (Johnson et al., 2011). Confocal imaging verified the presence of IQGAP1 in the nucleus of both NUGC4 and MKN45 cells (**Figure 2B**) and the interaction of nuclear IQGAP1 with hnRNPM *in situ* was confirmed using proximity ligation assays (PLA) (**Figure 2C-D).** Quantification of the PLA signal per cell confirmed that the interaction between the two proteins was clearly detectable in the nucleus of both cell lines. Some cytoplasmic interaction sites were also detected, but they were minor compared to the nuclear ones (**Figure 2C-D**) in agreement with the immunoprecipitation results from cytoplasmic extracts (**Figure S2B**).

Together these results demonstrate the RNA-independent, nuclear interaction between hnRNPM and IQGAP1 in gastric cancer cells where the levels of both proteins are significantly deregulated.

Nuclear IQGAP1-containing RNPs are involved in splicing regulation.

To identify other nuclear IQGAP1 interacting partners, we performed immunoprecipitation with anti-IQGAP1 Abs from nuclear extracts of NUGC4 cells and analysed the resulting proteins by LC-MS/MS (**Table S1**). GO-term enrichment analysis of the co-precipitated proteins showed a significant enrichment in biological processes relevant to splicing regulation (**Figure S3A**). Construction of an IQGAP1 interaction network revealed that IQGAP1 can interact not only with the majority of the hnRNPs, but also with a large number of spliceosome components (mainly of U2, U5snRNPs) and RNA-modifying enzymes (**Figure 3A**). The interactions between IQGAP1 and selected hnRNPs (A1, A2B1, C1C2, L, M) and with selected spliceosome components and RNA processing factors (SRSF1, CPSF6, DDX17, DHX9, ILF3/NF90) (Cvitkovic and Jurica, 2013) were independently validated in both NUGC4 and MKN45 cells (**Figure 3B, Figure S3B**). The interactions of IQGAP1 with hnRNPs A1, A2B1 are RNA-dependent, whereas only a subset of hnRNPs (L, C1/C2) interact with IQGAP1 in the absence of RNA (**Figure 3B**). These observations pinpointed to the interaction with hnRNPM as a distinct one, worthy of further investigation.

In the nuclear extracts used in our immunoprecipitations hnRNPM is enriched together with the majority of hnRNPs (Choi and Dreyfuss, 1984; Kafasla et al., 2000) (e.g. A2B1, K), other nuclear speckle components like SRSF1, and nuclear matrix associated proteins like SAFB and MATRIN3 (**Figure 3C and Figure S3C**), but not histones such as H3, which are present mainly in the insoluble nuclear material (**Figure S3C**). To further explore the interactions of nuclear IQGAP1 with the splicing machinery, we queried whether itself and its interacting partners are present in described splicing-related subnuclear fractions (Damianov et al., 2016). This was justified by the recent identification of hnRNPM as a significant component of the

Large Assembly of Spliceosome Regulators (LASR). This complex is assembled via protein-protein interactions, lacks DNA/RNA components, and appears to function in co-transcriptional AS (Damianov et al., 2016). In MKN45 cells, IQGAP1 and hnRNPM co-exist mainly in the soluble nuclear fraction together with hnRNPs K, C1/C2 and other spliceosome components (Damianov et al., 2016). Significantly smaller IQGAP1 and hnRNPM amounts were detected in the proteins released from the HMW material upon DNase treatment (D), together with hnRNPC1/C2 and other spliceosome components, including SF3B3 (**Figure 3D).** These results indicate that the interacting pools of IQGAP1 and hnRNPM are not major LASR components.

To assess the possible functional involvement of IQGAP1 in splicing, we used the hnRNPM responsive DUP51M1 and control DUP51-ΔM mini-gene reporters (Damianov et al., 2016). DUP51M1 is a three exon minigene, where the second exon contains a unique UGGUGGUG hnRNPM consensus binding motif, which results in exon 2 skipping in the presence of hnRNPM. All other potential binding sites have been mutated. The DUP51-ΔM minigene carries a mutation in the hnRNPM binding site. hnRNPM acts as a silencer for exon 2, as demonstrated by the marked increase in its inclusion in cells transfected with the DUP51-ΔM minigene or treated with *HNRNPM* siRNA compared to control cells (**Figure S4A-B).** Transfection with the pDUP51M1 plasmid and RT-PCR analysis resulted in different splicing patterns of the reporter in these cell lines: significantly more inclusion of exon 2 was detected in NUGC4, which express IQGAP1 at higher levels, than MKN45 (**Figure S4A)**. Moreover, the dependence of exon 2 inclusion of the DUP51-ΔM reporter on hnRNPM was more pronounced in MKN45 compared to NUGC4 (**Figure S4A)**. These results prompted us to focus on MKN45 cells to further probe the involvement of the hnRNPM-IQGAP1 interaction in AS. Using CRISPR-Cas9 genome editing we

knocked-out IQGAP1 in MKN45 cells without significant change in hnRNPM protein levels (**Figure 4A).** In this IQGAP1-KO background, the DUP51M1 reporter presented a significant ~2-fold increase in exon 2 inclusion compared to the parental cells (**Figure 4B-C)**. As expected from the interaction of IQGAP1 with other splicing factors (**Figure 3),** splicing of the DUP51-ΔM reporter was also affected upon IQGAP1 loss. However, this change was smaller (~1.3-fold increase) compared to the impact on hnRNPM-dependent splicing (**Figure 4B-C**). Attempts to restore splicing efficiency by expressing GFP-IQGAP1 were inconclusive, as the recombinant protein localized very efficiently in the nucleus (Johnson et al., 2011), thus inhibiting rather than rescuing exon 2 skipping (**Figure S4C**), likely due to sequestration of hnRNPM from the splicing machinery. The association of hnRNPM with this transcript *in vivo* was confirmed by crosslinking, immunoprecipitation with anti-hnRNPM, and RT-PCR of the associated pre-mRNA. The DUP51M1 transcript was detected at similar levels in the RNA crosslinked to hnRNPM in MKN45 and MKN45-*IQGAP1*^{KO} cells (**Figure 4D**). These results denote that IQGAP1 is required for hnRNPM splicing activity.

It is known that heat-shock alters the splicing activity of hnRNPM and its subnuclear localization. We assessed the role of IQGAP1 in such stress responses using staining for hnRNPM and IQGAP1 in MKN45 and MKN45-*IQGAP1*^{KO} cells before and after heat-shock. The MKN45 control cells showed the expected granular hnRNPM pattern on heat shock (Gattoni et al., 1996). Unexpectedly, hnRNPM localization and staining pattern did not change upon heat-shock in MKN45-*IQGAP1*^{KO} cells **(Figure 4E).** This was corroborated by nuclear matrix preparations, where hnRNPM was elevated in nuclear matrix of MKN45 cells after heat-shock compared to untreated cells, whereas this change was not detected in MKN45-*IQGAP1*^{KO} cells (**Figure 4F)**.

Interestingly, IQGAP1 levels were also increased in nuclear matrix fractions prepared from heat-shocked cells (**Figure 4F).** This prompted us to test the localization of IQGAP1 by confocal imaging, which revealed increased nuclear IQGAP1 staining in heat-shocked cells, compared to the untreated controls (**Figure S4D).** Collectively, these results indicate the involvement of IQGAP1 in spliceosomal nuclear RNPs, with a more significant role in regulating the splicing activity of hnRNPM.

A broad role of IQGAP1 in hnRNPM-dependent splicing.

To determine whether IQGAP1-KO results in broad splicing deregulation, we profiled AS changes between MKN45 and MKN45-*IQGAP1*^{KO} cells by RNA-seq (**Figure 5A-C)**. A number of significantly altered AS events were detected (**Figure 5A** and **Table S2A**) more than 50% of which were alternative exons (**Figure 5B)**. GO term enrichment analysis of the affected genes yielded significant enrichment of the biological processes of cell cycle (GO:0007049, *P*: 3.75E-04) and cell division (GO:0051301, *P*: 3.33E-04) (**Table S2B**). The presence of hnRNPM consensus binding motifs (Huelga et al., 2012) was significantly enriched downstream of 81% of the down-regulated alternative exons. Statistical analysis showed that down-regulated exons are more likely to have the hnRNPM binding motif than up-regulated exons (chi-square (1, 86) = 36.4848, $P < 0.00001$; **Figure 5C-D**). Therefore, the above indicate that IQGAP1 and hnRNPM co-operatively regulate the AS of a cell-cycle regulon.

Splicing events selected for validation were required to adhere to most of the following criteria: 1) high difference in Psi (ΔPsi) between the two cell lines (where [Psi] is the Percent Spliced In, i.e. the ratio between reads including or excluding exons), 2) involvement of the respective proteins in the cell cycle, 3) previous

characterization of pre-mRNAs as hnRNPM targets (Van Nostrand et al., 2016; Zhu et al., 2019) and/or 4) presence of the hnRNPM-consensus motif. 12 out of 19 AS events (63%) selected based on the above criteria were validated by RT-PCR **(Figures 5E, S5A-C, Table S3).**

ANAPC10 pre-mRNA was singled out for further analysis as it had the highest change in |ΔPsi|/Psi combination and it is a hnRNPM-eCLIP target (Van Nostrand et al., 2016) with the major hnRNPM binding sites downstream of the regulated exon, where the respective consensus binding motif is also located (**Figure S5D**). Importantly for cancer cells, ANAPC10 plays a crucial role in cell cycle and cell division (Alfieri et al., 2017; da Fonseca et al., 2011; Yamano, 2019; Zhou et al., 2016) as a substrate recognition component of the anaphase promoting complex/cyclosome (APC/C), a cell cycle-regulated E3-ubiquitin ligase that controls progression through mitosis and the G1 phase of the cell cycle. ANAPC10 interacts with the co-factors CDC20 and/or CDH1 to recognize targets to be ubiquitinated and subsequently degraded by the proteasome. In MKN45-*IQGAP1*^{KO} cells, increased levels of *ANAPC10* exon 4 skipping were detected (**Figure 5E**), an event predicted to result in an isoform lacking amino acid residues important for interaction with the D-box of its targets (Alfieri et al., 2017; da Fonseca et al., 2011). Knock-down of hnRNPM using siRNAs in MKN45-*IQGAP1*^{KO} led to an even higher increase in *ANAPC10* exon 4 skipping compared to scr-siRNA transfected cells (**Figure 5F**). These results denote that IQGAP1 interacts with hnRNPM in the nucleus of gastric cancer cells to generate an alternatively spliced isoform of, at least, ANAPC10 that, in turn, tags cell cycle-promoting proteins for degradation, thus contributing to the accelerated proliferation phenotype of these tumour cells.

To provide further evidence for this growth-promoting impact of the IQGAP1-hnRNPM interaction on gastric cancer cells, we determined whether *ANAPC10* exon 4 skipping results in decreased activity of the APC/C complex by comparing the proteomes of MKN45 and MKN45-*IQGAP1*^{KO} cell lines. Comparison of the levels of known targets of the APC/C complex in the two cell lines indicated increased abundance of the APC/C-CDH1 targets during anaphase (Zhou et al., 2016), RRM2, TPX2, ANLN, and TK1, but not of other APC/C known targets (**Figure S5E).** Immunoblotting showed that TPX2, RRM2 and TK1 levels were indeed increased in MKN45-*IQGAP1*^{KO} cells and even more in MKN45-*IQGAP1*^{KO} after siRNA mediated *hnRNPM* knock-down (**Figure 5G**). The same was true for CDH1/FZR, an APC/C co-factor, which is also a target of the complex, as is ANLN (**Figure S5F**). Interestingly, ANAPC10 levels were reduced in MKN45-*IQGAP1*^{KO} after knock-down of *hnRNPM*. Collectively, these results indicate that IQGAP1 interacts with hnRNPM to alter its splicing activity towards, at the very least, a gastric cancer growth-promoting form of the APC/C complex.

IQGAP1 and hnRNPM regulate gastric cancer cell growth *in vitro* and *in vivo*

To test the significance of IQGAP1 and hnRNPM in tumour development, we attempted to generate hnRNPM-KO cell lines and double KO for both hnRNPM and IQGAP1 using the CRISPR-Cas9 approach. Numerous attempts to disrupt the ORF of *hnRNPM* resulted in ~75% reduction, as we could not isolate single hnRNPM-KO clones. Thus, for the subsequent experiments we either worked with mixed cell populations (*MKN45-hnRNPM*^{KO}*-IQGAP1*^{KO}) with 75% reduced hnRNPM

expression levels (**Figure S6A**), or, where stated, we used siRNAs for down-regulation of the hnRNPM levels.

To evaluate the role of the two proteins in gastric cancer progression, we first assayed the parental and KO cell lines (MKN45-*IQGAP1*^{KO}, *MKN45-hnRNPM*^{KO} and *MKN45-hnRNPM*^{KO}*-IQGAP1*^{KO}) for cell growth and viability *in vitro*. In a 2D colony formation assay, cells with reduced levels of both interacting proteins generated significantly reduced number of colonies compared to parental cells (**Figure 6A).** Wound healing assays did not reveal significant differences in the migratory ability of these cell lines, only an increase in wound healing rate for MKN45-*hnRNPM*^{KO} cells compared to the parental line. Importantly, this expedited wound healing in MKN45-*hnRNPM*^{KO} cells was completely abolished upon concomitant absence of IQGAP1 (**Figure S6B).** Downregulation of both IQGAP1 and hnRNPM protein levels impairs also cellular metabolic activity, compared to the *IQGAP1*^{KO} and the parental lines, as indicated by MTT assays performed over a period of 5 days (**Figure 6B)**. However, we detected an increased metabolic rate in *IQGAP1*^{KO} cells, which can be attributed to hnRNPM-independent changes in metabolic activity in the absence of IQGAP1 (data not shown).

We then aimed to determine the impact of the two interacting proteins in gastric cancer progression based on the synergistic effect of IQGAP1 and hnRNPM on APC/C and its targets (**Figure 5**). To that end, we performed cell cycle analyses using propidium iodide-FACS. Unsynchronized MKN45-*IQGAP1*^{KO} cells showed a small but significant population increase at the S and G2/M phases with subsequent reduction of G1 cells (**Figure 6C**). MKN45-*hnRNPM*^{KO} cells showed a similar phenotype, whereas depletion of both interacting proteins (*MKN45-hnRNPM*^{KO}*-IQGAP1*^{KO}) enhanced the effect (**Figure 6C).** The population increase was stronger

after cell synchronization (**Figure S6C**). Given the role of APC/C and its targets, TK1, RRM2 and TPX2 in the progression of mitosis and cell division (Engström et al., 1985; Neumayer et al., 2014; Sherley and Kelly, 1988; Zhou et al., 2016), we investigated the double KO cells (*MKN45-hnRNPM*^{KO}*-IQGAP1*^{KO}) for deficits in cell division. DAPI staining and anti-β-tubulin cytoskeleton immunostaining revealed significant number of MKN45-*IQGAP1*^{KO}*-hnRNPM*^{KO} cells being multinucleated (2 or more nuclei; **Figure 6D-E)**. A similar phenotype was detected when we used siRNAs to downregulate hnRNPM levels (**Figure S6D**).

To examine the *in vivo* effect of abrogating *IQGAP1* and *hnRNPM* on tumour development and progression, we injected MKN45, MKN45-*IQGAP1*^{KO}, *MKN45-hnRNPM*^{KO} and *MKN45-hnRNPM*^{KO}*-IQGAP1*^{KO} cells subcutaneously into the flanks of NOD/SCID mice. Measurements of tumour dimensions throughout the experiment demonstrated that cells lacking both IQGAP1 and hnRNPM present significantly reduced tumour growth compared to the parental MKN45 and the single KO cells (**Figure 7A**). Immunohistochemical analysis of the tumours confirmed greatly reduced levels of hnRNPM and/or IQGAP1 in the mutant cell line-derived xenografts. Furthermore, Ki-67 staining was highly reduced in the single and double KO tumours compared to the parental cell line-derived ones, showing the involvement of the two proteins in the *in vivo* proliferation of gastric cancer cells (**Figure 7B)**. Collectively, these results demonstrate that co-operation of IQGAP1 and hnRNPM is required for gastric cancer growth and progression.

Discussion

Splicing regulatory networks are subject to signals modulating alternative exon choice. One of the best characterized AS changes in response to stress-signals is the shutdown of post-transcriptional pre-mRNA splicing observed in heat-shocked cells (Biamonti and Caceres, 2009; Shalgi et al., 2014). However, how this occurs mechanistically is still unknown. Here, we report the first insights for the roles of hnRNPM and IQGAP1 in mediating the response of the spliceosome to heat-induced stress (Gattoni et al., 1996). The fact that IQGAP1 is a scaffold protein with well-known roles in the cytoplasm as an integrator of many signalling cascades suggests that this may be a more general phenomenon. We show that in gastric cancer cells, the interaction of the two proteins is necessary for the response of hnRNPM to heat-induced stress signals. Furthermore, we show here that nuclear IQGAP1 interacts with a large number of splicing regulators mostly in an RNA-dependent manner, in addition to its RNA-independent interaction with hnRNPM. Thus, based on our data, we propose that upon heat, and possibly other stressors, IQGAP1 and hnRNPM are removed from the spliceosome and move towards the less-well-defined nuclear matrix. IQGAP1 is not required for binding of hnRNPM to a reporter pre-mRNA *in vivo*, however, it is necessary for the function of hnRNPM in splicing, possibly regulating the interaction of hnRNPM with spliceosomal components at distinct subnuclear compartments.

The nuclear translocation and localization of IQGAP1 appears to be cell-cycle dependent, since it is significantly increased in response to replication stress and subsequent G1/S arrest (Johnson et al., 2011) and as presented herein, upon heat-shock. This finding complements prior reports suggesting IQGAP1 localization at the nuclear envelope during late mitotic stages (Lian et al., 2015). Cyclebase data (Santos

et al., 2015) suggest that hnRNPM is required for progression of the cell cycle G1 phase. On the basis of our data, we propose that in the absence of IQGAP1, a number of pre-mRNAs involved in cell cycle regulation undergoes altered alternative splicing.

IQGAP1 and hnRNPM seem to co-operatively regulate the AS of a cell-cycle regulon. Specifically, 5 out of the 10 cell division-related AS events that are deregulated in the absence of IQGAP1 are exon skipping events, characterized by the presence of the hnRNPM binding motif downstream of the alternative exon. Of these 5 events, ANAPC10 has the highest change in AS pattern upon IQGAP1 abrogation and a significant role in cell cycle regulation and cell division (Yamano, 2019; Zhou et al., 2016). In cells with reduced amounts of both IQGAP1 and hnRNPM, ANAPC10 levels are reduced and at least a group of APC/C-CDH1 targets are specifically stabilized (TPX2, RRM2, TK1, CDH1 itself). Given the role of the controlled degradation of these proteins for cell cycle progression (Penas et al., 2011; Zhou et al., 2016), we posit that these observations explain the aberrant cell cycle effect in the double KO cell lines, the multinucleated cells phenotype and the importance of the two proteins for gastric cancer development and progression as detected by the xenograft experiments.

Currently, the literature on cell cycle control, multinucleated cancer cells and tumour growth is rather unclear and often conflicting. There is evidence connecting these cell cycle effects manifested as a balance between up-regulation or down-regulation of tumour growth (Gijn et al., 2019; Levine and Holland, 2018; Penas et al., 2011; Sansregret et al., 2017). Mitotic errors, such as mitotic exit defects can have distinct impacts at different points during tumour development (Penas et al., 2011). Thus, targeting of the APC/C^{Cdh1} activity has been suggested as a possible tumour suppressive approach (Penas et al., 2011; Yamano, 2019). Our data put these

phenotypes into context, leading to an experimentally testable model in which IQGAP1 and hnRNPM co-operatively drive this balance towards tumour growth, and when they cannot interact, the balance is shifted towards tumour suppression. They accomplish this by adding a new level of control in the activity of the APC/C complex: alternative splicing regulation. If so, it is of critical importance to identify additional protein partners involved in this balancing mechanism and investigate whether this mechanism is involved both in additional cancer types and also in normal cells.

Acknowledgements:

We thank N. Boni-Kazantzidou (Centre for Proteome Research, Liverpool, UK) and G.-R. Manikas (European Commission, Brussels, Belgium) for the generation of crucial preliminary data; P. Hantzis, M. Fousteri, V. Koliaraki (Institute for Fundamental Biomedical Research, B.S.R.C. “Al. Fleming”), A. Skorilas (Dept. of Biology, University of Athens, Greece) and N. Balatsos (Dept. of Biochemistry and Biotechnology, University of Thessaly, Greece) for cell lines and reagents; D. Black and A. Damianov (Department of Microbiology, Immunology, and Molecular Genetics, UCLA, USA) for plasmids and technical advice on minigene reporter splicing assays; A. Guialis (N.H.R.F., Athens, Greece) for antibodies and reagents; Per Haberkant, Frank Stein and the EMBL Proteomics Core Facility for LC-MS/MS analyses and advise; Sofia Grammenoudi and the Flow cytometry facility of B.S.R.C. “Al. Fleming” for help with cell cycle analyses and disussions; Vladimir Benes, Jonathan Landry and the EMBL Genecore for RNA-seq analyses and discussions; Martina Samiotaki, George Stamatakis at the Proteomics Facility of B.S.R.C. “Al.

Fleming" for LC-MS/MS analyses and discussions. We also thank George Panayotou and Efthimios Skoulakis (B.S.R.C. "Al. Fleming") for critical reading of the manuscript; Juan Valcarcel for help with the analysis of the RNA-seq data; Skarlatos G. Dedos (Department of Biology, National and Kapodistrian University of Athens, Greece) for reagents, plasmids, discussions and critical reading of the manuscript.

A.B. was supported by InfrafrontierGR/Phenotypos (MIS 5002135) and by the start-up fund of P.K. M.P. was supported by the start-up fund of P.K.. V.P. and Z.E. were supported by the Hellenic Foundation for Research & Innovation (HFRI) and the General Secretariat for Research and Technology (GSRT) to Z.E., under grant agreement 846. J.L. was supported by EMBL Core Facilities. M.R. was supported by the European Research Council (ERC AdvG 670146). M.A. and D.K were supported by InfrafrontierGR/Phenotypos (MIS 5002135). This work was funded by a European Commission Grant FP7-PEOPLE-2010-IEF (274837) to P.K and was supported by a start-up fund to P.K. from a Stavros Niarchos Foundation donation to BSRC "Al. Fleming" and by the Hellenic Foundation for Research & Innovation (HFRI) and the General Secretariat for Research and Technology (GSRT), under grant agreement 846.

Author contributions

These authors contributed equally: Andrada Birladeanu, Malgorzata Rogalska, Myrto Potiri.

A.B. performed most of the immunofluorescence, subcellular fractionation, immunostaining and *in vitro* splicing experiments. M.R. performed all the statistical and bioinformatics analyses. M.P. performed the cellular assays (cell cycle, wound

healing, colony formation, MTT assays). Z.E. performed RT-PCR analyses and supervised A.B in *in vitro* splicing assays and M.P in cell cycle analyses and edited the manuscript. V.P. performed immunofluorescence analyses, western blotting analyses, advised A.B. on image acquisition and analyses, supervised M.P. on cellular assays and edited the manuscript. M.A. and P.K. performed the xenograft experiment. D.K. advised M.A. and helped with the cellular assays. J.D.L. advised and edited the manuscript. P.K conceived, designed and supervised the study, performed the immunoprecipitation experiments and wrote the manuscript. All authors commented on the manuscript.

Declaration of Interests

The authors declare no competing interests.

Figure Legends

Figure 1: hnRNPM and IQGAP1 expression levels are altered in gastric cancer. (A) Representative epifluorescence images of normal and adenocarcinoma gastric tissues on a commercial tissue microarray. Tissues were immunostained with mouse anti-hnRNPM and rabbit anti-IQGAP1 antibodies. DAPI was used for nuclei staining. The same settings for hnRNPM and IQGAP1 signal acquisition were applied in all samples. **(B)** Expression matrix plot showing the *IQGAP1* and *HNRNPM* mRNA levels in tumour samples (T) from Stomach Adenocarcinoma (STAD) patients in comparison to TCGA normal and GTex data. The density of colour in each block represents the median expression value of a gene in a given tissue, normalized by the maximum median expression value across all blocks. The expression levels are

indicated in $\log_2$(TPM + 1) values. The plot was generated using the gepia2 website (http://gepia2.cancer-pku.cn/#indexn). Sample numbers: 408 tumours, 36 normal and 175 stomach GTex. **(C)** Correlation plots of the expression of *hnRNPM* and *IQGAP1* mRNAs in normal gastric tissues (GTEx database), normal-adjacent tissues (TCGA STAD Normal database) and tumours from Stomach Adenocarcinoma (STAD) patients (TCGA STAD Tumour database). The plots were generated using the gepia2 website. R: Spearman correlation coefficient. Sample numbers were as in (**B**). **(D)** Immunoblotting of crude protein extracts from different gastric cancer cell lines against hnRNPM and IQGAP1. β-actin was used to normalize hnRNPM and IQGAP1 levels. MKN45 cells were used as a reference for the comparison of the expression levels between cell lines (ratios shown at the bottom). Quantification was performed using ImageLab software version 5.2 (Bio-Rad Laboratories). AGS: gastric adenocarcinoma; MKN45: poorly differentiated gastric adenocarcinoma, liver metastasis; KATOIII: gastric carcinoma, pleural effusion and supraclavicular and axillary lymph nodes and Douglas cul-de-sac pleural; NUGC4: poorly differentiated gastric adenocarcinoma, gastric lymph node.

Figure 2. IQGAP1 and hnRNPM interact in the nucleus of gastric cancer cell lines. (A) Immunoprecipitation using an anti-IQGAP1 antibody or control IgG using nuclear extracts from MKN45 and NUGC4 cells, in the presence or absence of RNase A (0.1 mg/ml for 30 min). Immunoblot detection of IQGAP1 and hnRNPM is shown in comparison to 1/70th of the input used. **(B)** Representative confocal images of MKN45 and NUGC4 cells stained with an anti-IQGAP1 antibody and DAPI to visualise the nuclei. Single confocal slices are shown for each fluorescence signal and for the merged image. Cross sections of the xz and yz axes show the presence of IQGAP1 within the cell nuclei. (**C-D**) Proximity ligation assay (PLA) in MKN45 and

NUGC4 cells showing the direct nuclear interaction between hnRNPM and IQGAP1. Representative images for the 2 cell lines displaying a central plane from confocal z-stacks are shown in **(C)**. Negative control (secondary antibody only, MKN45 C and NUGC4 C) samples show minimal background signal. **(D)** Quantification of the nuclear (n.MKN45 and n.NUGC4) and cytoplasmic signal (c.MKN45 and c.NUGC4) was performed per cell, using the DuoLink kit-associated software. Each plot represents at least 15 cells analysed. *P* values were calculated using ANOVA multiple comparisons tests; ****$P < 0.0001$.

Figure 3. **Nuclear IQGAP1 participates in RNPs together with a large number of RNA-processing factors in gastric cancer cell lines**. **(A)** Network of protein interactions generated from the proteins that were pulled down by anti-IQGAP1 from nuclear extracts of NUGC4 cells classified as spliceosomal components. The network was generated using the igraph R package. Colours represent classes of spliceosomal components according to SpliceosomeDB (Cvitkovic and Jurica, 2013). Vertices are scaled according to *P* values and ordered according to known spliceosomal complexes. **(B)** Validation of representative IQGAP1-interacting partners presented in (**A**). Anti-IQGAP1 or control IgG pull down from nuclear extracts of NUGC4 and MKN45 cells were immunoprobed against IQGAP1, hnRNPA1, hnRNPA2/B1, hnRNPC1/C2, hnRNPL and DHX9/RHA. The immunoprecipitated proteins were compared to 1/70th of the input used in the pull down. Where indicated, RNase A was added in the pull down for 30 min. Numbers indicate MW in kDa. **(C)** Subcellular distribution of hnRNPM and IQGAP1. MKN45 and NUGC4 cells were subjected to subcellular fractionation as described in Online Methods. Equal amounts of the resulting cytosolic and soluble nuclear fractions as well as the insoluble nuclear material were analysed by Western blot for the presence of IQGAP1, hnRNPM,

hnRNPA2/B1 and SRSF1. Lamin b1 and β-actin were used as fractionation and loading controls, respectively. Numbers indicate MW in kDa. **(D)** Subnuclear distribution of hnRNPM and IQGAP1. Soluble and High Molecular Weight (HMW) nuclear extracts from MKN45 cells were prepared as described in Online Methods. Protein complexes from the HMW fraction were released after treatment with DNase (D) or RNase (R). Equal amounts of all fractions were analyzed by Western blot for the presence of IQGAP1, hnRNPM, hnRNPK/J, hnRNPC1/C2 and SF3B3. Numbers indicate MW in kDa.

Figure 4. Nuclear IQGAP1 significantly affects hnRNPM-dependent splicing. (A) Immunoblot of MKN45 whole-cell lysates showing the effective reduction of IQGAP1 protein levels after CRISPR/Cas9 genome editing. β-actin was used as loading control. **(B-C)** Involvement of IQGAP1 in hnRNPM-dependent AS. MKN45 and MKN45-*IQGAP1*^{KO} cells were transfected with the DUP51M1 or DUP51ΔM1 minigene splicing reporters (Damianov et al., 2016) for 40 hrs. Exon 2 (grey box) splicing was assessed by RT-PCR using primers located at the flanking exons. Spliced products are shown in **(B)**. Quantification of exon 2 inclusion **(C)** was performed using ImageJ. Data shown represent the average exon 2 inclusion values ± SD from at least 3 independent experiments. *P* values were calculated using unpaired, two-tailed, unequal variance Student´s t-test. **(D)** As in (B) cells transfected with DUP51M1 minigene were UV cross-linked and lysed under denaturing conditions. RNA:protein crosslinks were immunoprecipitated with an anti-hnRNPM antibody. hnRNPM, GAPDH in the lysates (lanes: input) and immunoprecipitates (lanes: IP) were detected by immunoblot. RT-PCR was used to detect DUP51M1 pre-mRNA and GAPDH mRNA. Graph shows the amounts of co-precipitated RNA normalised to the IgG negative control and to the amount of hnRNPM protein that was pulled-down in each

IP. Bars represent mean values ± SD from 3 independent experiments. **(E)** Representative images of MKN45 and MKN45-*IQGAP1*^{KO} cells stained for hnRNPM, IQGAP1 and DAPI after heat-shock stress induction for 15 min at 45°C. **(F)** Immunoblot of nuclear matrix extracts from cells shown in (E), exhibiting the increase of hnRNPM protein localisation in the nuclear matrix upon heat-shock. β-actin is used as a loading control (Rando et al., 2000). Quantification of the relevant amounts, in arbitrary units, was performed using ImageLab software version 5.2 (Bio-Rad Laboratories).

Figure 5. IQGAP1 regulates alternative splicing of a cell cycle-related regulon. **(A)** Scatterplot with the distribution of the Psi values for the AS events detected by VAST-TOOLS in RNA-seq in IQGAP1KO and control cells. In yellow are the significantly changed AS events between MKN45 and MKN45-*IQGAP1*^{KO} cells (|ΔPsi|>15, range 5), in ochre and orange are events with detected iClip binding for hnRNPM or predicted RNA-binding motif, respectively. The gene names of the events that were selected for validation are indicated. In bold are representative events related to cell cycle (GO:0007049) (see also **Table S3**). BG: background. **(B)** Pie chart presenting the frequency of the different types of AS events (exon skipping, intron retention, alternative splice donor and alternative splice acceptor) regulated by IQGAP1 in MKN45 cells. **(C)** Classification of the up-regulated (Up) and down-regulated (Down) exons in MKN45-*IQGAP1*^{KO} cells compared to MKN45, as i. having the hnRNPM consensus binding motif downstream of the regulated exon, ii. having been identified as iCLIP targets, iii. belonging to both (i.) and (ii.) and iv. not belonging in any of the above categories. **(D)** Schematic showing the position of the hnRNPM binding motif enrichment relative to the alternatively spliced exon (grey box). The reported hnRNPM motifs (Huelga et al., 2012) were identified only down-

stream of the down-regulated exons. **(E)** *IQGAP1*^{KO} affects AS of *ANAPC10* in MKN45 cells, by promoting exon 4 skipping. RT-PCR (see **Table S4**) followed by electrophoresis were used to monitor the rate of *ANAPC10* exon 4 inclusion in MKN45 and MKN45-*IQGAP1*^{KO} cells. Exon 4 inclusion was quantified with ImageJ in at least 3 biological replicates. *P* value was calculated with unpaired *t*-test. **(F)** *ANAPC10* exon 4 inclusion was analysed in MKN45 and MKN45-*IQGAP1*^{KO} cells transfected with siRNAs for hnRNPM or scrambled (scr) control siRNAs, as described in **(E). (G)** Immunoblot analysis to monitor the steady-state levels of TPX2 (2 isoforms), RRM2 and TK1 in crude protein extracts from MKN45 and MKN45-*IQGAP1*^{KO} cells transfected with siRNAs for hnRNPM or scrambled control (scr) as indicated. *IQGAP1*^{KO} and the efficiency of hnRNPM down-regulation were also confirmed by immunoblotting. β-actin was used as loading control for the TK1 immunoblot and GAPDH was the loading control for all other immunoblots shown. Numbers indicate MW in kDa.

Figure 6. hnRNPM and IQGAP1 act co-operatively to regulate cell division and tumour growth *in vitro*. Analysis of MKN45, MKN45-*IQGAP1*^{KO}, MKN45-*hnRNPM*^{KO} and double MKN45-*IQGAP1*^{KO}-*hnRNPM*^{KO} cells using *in vitro* assays. **(A)** 2D colony formation assays to measure the ability of the different cell lines to form colonies. Bar graph shows the average fold difference ± SD between the numbers of colonies formed across the different groups from 3 independent experiments. *P*-values were calculated using two-tailed, unpaired t-tests, where $*P < 0.05$, $***P < 0.001$. Representative images for each cell line are shown at the bottom. **(B)** MTT cell proliferation assays to measure the metabolic activity of the 4 cell lines. Growth curves show the mean absorbance values/day from 3 independent experiments. *P* values were calculated using two-tailed, unpaired t-tests, where $**P <$

0.01. **(C)** Cell cycle analysis of asynchronous MKN45-derived cell lines using propidium iodide staining followed by FACS analysis. Quantification of the percentage of cells in each cell cycle phase was performed with FlowJo software. Data represent mean values ± SD of two independent experiments. ***$P < 0.001$, ****$P < 0.0001$. (**D-E)** Non-synchronized cells from all four cell groups were stained for β-tubulin and DAPI, to visualize the cell cytoplasm and nucleus, respectively. A representative confocal image of the double MKN45-*IQGAP1*^{KO}-*hnRNPM*^{KO} stained cells in **(D)** shows the pronounced multi-nucleation observed in these cells. Quantification of the percentage of cells having 1x, 2x or >2x nuclei (**E**) was performed in 20 images from each cell line, reaching a minimum number of 250 cells analysed per group.

Figure 7. hnRNPM and IQGAP1 act co-operatively to regulate tumour growth *in vivo*. MKN45, MKN45-*IQGAP1*^{KO}, *MKN45-hnRNPM*^{KO} and *MKN45-hnRNPM*^{KO}-*IQGAP1*^{KO} cells were subcutaneously injected into the flanks of NOD/SCID mice and tumours were left to develop over a period of 28 days. **(A)** The tumour growth graph shows the increase of tumour volume (mm^3) over time. Tumour size was measured in anesthetised mice with a digital caliper twice per week, and at the end-point of the experiment when tumours were excised. Data presented are average values ± SD, from 11 mice per group. *P* values were calculated using one-way ANOVA, where *$P < 0.05$, **$P < 0.01$, ****$P < 0.0001$. **(B)** Excised tumours from all four cell lines were embedded in paraffin, sectioned and stained for H&E and also probed with antibodies against hnRNPM, IQGAP1 and Ki67. Representative pictures from one tumour from every cell group are shown, displaying reduced levels of IQGAP1 and hnRNPM in MKN45-*IQGAP1*^{KO} and *MKN45-hnRNPM*^{KO} derived tumours respectively, while staining for both proteins is reduced in the double *MKN45-hnRNPM*^{KO}-*IQGAP1*^{KO}

tumours. The latter samples are also characterised by a marked decrease in Ki-67 staining, demonstrating the cooperative effect of hnRNP and IQGAP1 in *in vivo* tumour proliferation.

Supplemental Tables

Table S1. (Related to Figure 3 and Figure S3)

Data generated from the analysis of the anti-IQGAP1 immunoprecipitation samples by LC-MS/MS.

Table S2 (Related to Figure 5 and Figure S5)

a, Alternative splicing events identified to be significantly different between MKN45 and MKN45-*IQGAP1*^{KO} cells.

b, Biological process enrichment analysis of the differential alternative splicing events presented in **a.**

DATA AND CODE AVAILABILITY

The mass spectrometry proteomics data have been deposited to the ProteomeXchange Consortium via the PRIDE[69] partner repository with the dataset identifier XXXXXXXX.

RNA-seq data have been deposited in GEO: XXXXXXXXX.

MATERIALS AND METHODS

In Vivo Animal Studies

All animal experiments were performed in the animal facilities of Biomedical Sciences Research Center (BSRC) "Alexander Fleming" and were approved by the Institutional Committee of Protocol Evaluation in conjunction with the Veterinary Service Management of the Hellenic Republic Prefecture of Attika according to all current European and national legislation and performed in accordance with the guidance of the Institutional Animal Care and Use Committee of BSRC "Alexander Fleming". Mice were housed in an area free of pathogens as defined by FELASA recommendations in IVC ages at 5 per cage at constant temperature (19-23^{0}C) and humidity (55% ± 10%), with a 12-hour light/dark cycle (lights on at 7:00 am) and were allowed access to food and water ad libitum. Mice were allowed to acclimatize for at least 7 days prior to the experiment and were randomly assigned to experimental groups. Both male and female mice were used, roughly matched between CTR and KO groups. Mice had not been involved in any previous procedures.

Mouse Xenograft studies

1 x10^{6} cells in 100μl of PBS:Matrigel (1:1; Corning) of MKN45, MKN45-IQGAP1^{KO}, MKN45-hnRNP-M^{KO} or double KO cells were injected into the flank of 8-10-week-old NOD-SCID. Groups of 11 mice were used per cell type, based on power analysis performed using the following calculator: https://www.stat.ubc.ca/~rollin/ stats/ssize/n2.html. Tumour growth was monitored up to 4 weeks and recorded by measuring two perpendicular diameters using the formula

1/2(Length × Width^2) bi-weekly (Euhus et al., 1986). At end-point, mice were euthanized and tumours were collected and enclosed in paraffin for further analyses.

Cell cultures

The human gastric cancer cell lines AGS, KATOIII, MKN45 and NUGC4 were a kind gift from P. Hatzis (B.S.R.C. "Al. Fleming", Greece). Cells were grown under standard tissue culture conditions (37^{0}C, 5% CO2) in RPMI medium (GIBCO), supplemented with 10% FBS, 1% sodium pyruvate and 1% penicillin–streptomycin. NUGC4 originated from a proximal metastasis in paragastric lymph nodes, and MKN45 was derived from liver metastasis. According to the GEMiCCL database, which incorporates data on cell lines from the Cancer Cell Line Encyclopedia, the Catalogue of Somatic Mutations in Cancer and NCI60 (Jeong et al., 2018), none of the gastric cancer cell lines tested have altered copy number of hnRNPM or IQGAP1. Only NUGC4 has a silent mutation c.2103G to A in *HNRNPM*, which is not included in the Single Nucleotide Variations (SNVs) or mutations referred by cBioportal in any cancer type (Cerami et al., 2012; Gao et al., 2013).

Transfection of MKN45 and NUGC4 cells

Gastric cancer cell lines were transfected with plasmids pDUP51M1 or pDUP51-ΔM (a gift from D. L. Black, UCLA, USA) and pCMS-EGFP (Takara Bio USA, Inc) or pEGFP-IQGAP1 (Ren et al., 2005) [a gift from David Sacks (Addgene plasmid # 30112; http://n2t.net/addgene:30112; RRID:Addgene_30112)], using the TurboFect transfection reagent (Thermo Fisher Scientific, Inc., MA). For RNA-mediated

interference, cells were transfected with control siRNA (sc-37007, Santa Cruz Biotechnology, Inc., CA) or hnRNPM siRNA (sc-38286) at 30 nM final concentration, using the Lipofectamine RNAiMAX transfection reagent (Thermo Fisher Scientific), according to manufacturer's instructions.

Subcellular fractionation

The protocol for sub-cellular fractionation was as described before (Kafasla et al., 2000). Briefly, for each experiment, approximately $1.0x10^7$-$1.0x10^8$ cells were harvested. The cell pellet was re-suspended in 3 to 5 volumes of hypotonic Buffer A (10 mM Tris-HCl, pH 7.4, 100 mM NaCl, 2.5 mM $MgCl_2$) supplemented with 0.5 % Triton X-100, protease and phosphatase inhibitors (1 mM NaF, 1 mM Na_3VO_4) and incubated on ice for 10 min. Cell membranes were sheared by passing the suspension 4-6 times through a 26-gauge syringe. Nuclei were isolated by centrifugation at 3000 x g for 10 min at 4^oC, and the supernatant was kept as cytoplasmic extract. The nuclear pellet was washed once and the nuclei were resuspended in 2 volumes of Buffer A and sonicated twice for 5s (0.2A). Then, samples were centrifuged at 4000 x g for 10 min at 4^oC. The upper phase, which is the nuclear extract, was collected, while the nuclear pellet was re-suspended in 2 volumes of 8 M Urea and stored at -20^oC. Protein concentration of the isolated fractions was assessed using the Bradford assay (Bradford, 1976).

For the subnuclear fractionation protocol that allows for analysis of the LASR complex (Damianov et al., 2016) cells were harvested, incubated on ice in Buffer B (10 mM HEPES-KOH pH 7.5, 15 mM KCl, 1.5 mM EDTA, 0.15 mM spermine) for 30 min and lysed with the addition of 0.3 % Triton X-100. Nuclei were collected by centrifugation and further purified by re-suspending the pellet in S1 buffer (0.25M

Sucrose, 10 mM $MgCl_2$) and laid over an equal volume of S2 buffer (0.35 M Sucrose, 0.5 mM $MgCl_2$). Purified nuclei were lysed in ten volumes of ice-cold lysis buffer (20 mM HEPES-KOH pH 7.5, 150 mM NaCl, 1.5 mM $MgCl_2$, 0.5 mM DTT and 0.6 % Triton X-100) and nucleosol was separated via centrifugation from the high molecular weight fraction (pellet). The high molecular weight (HMW) fraction was subsequently resuspended in Buffer B and treated with either DNase I (0.1 mg/ml) or RNase A (0.1 mg/ml). The supernatant was collected by centrifugation at 20,000 x g for 5 min, as the HMW treated sample.

The nuclear matrix fractionation was as previously described (Mähl et al., 1989). Briefly, cells were harvested and washed with PBS. The cell pellet obtained was re-suspended in a five packed cell pellet volumes of buffer A (10 mM Tris-HCl pH 7.5, 2.5 mM $MgCl_2$, 100 mM NaCl, 0.5% Triton X-100, 0.5 mM DTT and protease inhibitors) and incubated on ice for 15 min. The cells were then collected by centrifugation at 2000rpm for 10 min and re-suspended in 2 volumes of buffer A. To break the plasma membrane a Dounce homogenizer (10 strokes) was used and the cells were checked under the microscope. After centrifugation at 2000 rpm for 5 min, supernatant was gently removed and kept as cytoplasmic fraction, while the pellet containing the nuclei was re-suspended in 10 packed nuclear pellet volumes of S1 solution (0.25 M sucrose, 10 mM $MgCl_2$), on top of which an equal volume of S2 solution (0.35 M sucrose, 0.5 mM $MgCl_2$) was layered. After centrifugation at 2800 x g for 5 min, the nuclear pellet was re-suspended in 10 volumes of buffer NM (20 mM HEPES pH 7.4, 150 mM NaCl, 2.5 mM $MgCl_2$, 0.6 % Triton X-100 and Protease inhibitors) and lysed on ice for 10 minutes, followed by centrifugation as above. The supernatant was removed and kept as nuclear extract while the pellet was re-suspended in buffer A containing DNase I (0.5mg/mL) or RNase A (0.1 mg/mL) and

Protease inhibitors and stirred gently at room temperature for 30 minutes. The upper phase defining the nuclear matrix fraction was quantified and stored at -20˚C.

Immunoprecipitation

Co-immunoprecipitation of proteins was performed using Protein A/G agarose beads (Protein A/G Plus Agarose Beads, Santa-Cruz Biotechnologies, sc-2003) as follows: 20 μl of bead slurry per immunoprecipitation reaction was washed with NET-2 buffer (10 mM Tris pH 7.5, 150 mM NaCl, 0.05 % NP-40). 4-8 μg of antibody were added to a final volume of 500-600 μL in NET-2 buffer per sample. Antibody binding was performed by overnight incubation at 4°C on a rotating wheel. Following the binding of the antibody, beads were washed at least 3 times by resuspension in NET-2. For each IP sample, 500-1000 μg of protein were added to the beads, in a final volume of 800 μL with NET-2 buffer and incubated for 2 hrs at 4°C on a rotating wheel. After sample binding, beads were washed 3 times with NET-2 buffer, and twice with NET-2 buffer supplemented with 0.1% Triton X-100 and a final concentration of 0.1% NP-40. For the UV-crosslinking experiments, beads were washed five times with wash buffer containing 1M NaCl and twice with standard wash buffer. Co-immunoprecipitated proteins were eluted from the beads by adding 15-20 μL of 2x Laemmli sample buffer (0.1 M Tris, 0.012% bromophenol blue, 4 % SDS, 0.95 M β-mercapthoethanol, 12 % glycerol) and boiled at 95°C for 5 min. Following centrifugation at 10.000 x g for 2 min, the supernatant was retained and stored at -20°C or immediately used.

Western Blot analysis

Cell lysate (7-10 μg for nuclear lysates and 15-20 μg for the cytoplasmic fraction) was resolved on an 8%, 10% or 12 % SDS-polyacrylamide gel and transferred to a

polyvinylidinedifluoride membrane (PVDF, Millipore). Primary antibodies were added and the membranes were incubated overnight at 4˚C. Antibodies were used against: hnRNPM (1:500, clone 1D8, sc-20002), IQGAP1 (1:1000, clone H109, sc-10792; 1:1000, clone C-9, sc-379021; 1:1000 clone D-3, sc-374307, all from Santa Cruz), beta-actin (1:1000, clone 7D2C10, 60008-1-Ig, ProteinTech), Lamin B1 (1:1000, clone A-11, sc-377000, Santa Cruz), GAPDH (1:2000, 60004-1-Ig, ProteinTech), hnRNP A2/B1 (1:1000, clone DP3B3, sc-32316, Santa Cruz), SRSF1 (SF2/ASF; 1:1000, SC-33652, Santa Cruz), hnRNP A1 (1:1000, clone 4B10, sc-32301, Santa Cruz), hnRNPL (1:1000, clone 4D11, sc-32317, Santa Cruz), hnRNP C1/C2 (1:1000, clone 4F4, sc-32308, Santa Cruz), DHX9/RHA (1:1000, ab26271, Abcam), hnRNP K/J (1:1000, clone 3C2, sc-32307, Santa Cruz), SF3B3 (1:1000, clone B-4, sc-398670, Santa-Cruz), beta tubulin (1:1000, clone 2-28-33, Sigma-Aldrich), TPX2 (1:200, clone E-2, sc-271570, Santa Cruz), RRM2 (1:200, clone A-5, sc-398294, Santa Cruz), SAFB (1:1000, F-3, sc-393403, Santa Cruz), Matrin3 (1:1000, 2539C3a, Santa Cruz), Histone-H3 (1:2000, 17168-AP, ProteinTech), DDX17 (clone H-7, sc-398168, Santa Cruz), CPSF6 (1:1000, sc-292170, Santa Cruz), NF90 (1:1500, clone A-3, sc-377406, Santa Cruz), anillin (1:1000, CL0303, ab211872, Abcam) , FZR (1:200, clone DCS-266, sc-56312, Santa Cruz), TK1 (1:5000, clone EPR3193, ab76495, Abcam), ANAPC10 (1:100, clone B-1, sc-166790, Santa Cruz). HRP-conjugated goat anti-mouse IgG (1:5000, 1030-05, SouthernBiotech) or HRP-conjugated goat anti-rabbit IgG (1:5000, 4050-05, SouthernBiotech) were used as secondary antibodies. Detection was carried out using Immobilon Crescendo Western HRP substrate (WBLUR00500, Millipore).

Generation of knockouts

The CRISPR/Cas9 strategy was used to generate IQGAP1 knockout cells (Ran et al., 2013). Exon1 of the *IQGAP1* transcript was targeted using the following pair of synthetic guide RNA (sgRNA) sequences: Assembly 1: 5'-CACTATGGCTGTGAGTGCG-3' and Assembly 2: 5'-CAGCCCGTCAACCTCGTCTG-3'. The sequences were identified using the CRISPR Design tool (Ran et al., 2013). These sequences and their reverse complements were annealed and ligated into the BbSI and BsaI sites of the All-In-One vector [AIO-Puro, a gift from Steve Jackson (Addgene plasmid #74630; http://n2t.net/addgene:74630; RRID:Addgene_74630)] (Chiang et al., 2016). The two pairs of complementary DNA-oligos (Assemblies 1 and 2 including a 4-mer overhang + 20-mer of sgRNA sequence) were purchased from Integrated DNA technologies (IDT). The insertion of sgRNAs was verified via sequencing. MKN45 and NUGC4 cells were transfected using Lipofectamine 2000, and clones were selected 48 h later using puromycin. Individual clones were plated to single cell dilution in 24 well-plates, and IQGAP1 deletion was confirmed by PCR of genomic DNA using the following primers: Forward: 5'-GCCGTCCGCGCCTCCAAG-3'; Reverse: 5'-GTCCGAGCTGCCGGCAGC-3' and sequencing using the Forward primer. Loss of IQGAP1 protein expression was confirmed by Western Blotting. MKN45 and NUGC4 cells transfected with AIO-Puro empty vector were selected with puromycin and used as a control during the clone screening process.

For the generation of the *hnRNPM* KO cells we used a different approach. We ordered a synthetic guide RNA (sgRNA) (5'- CGGCGTGCCGAGCGGCAACG-3'), targeting exon 1 of the *hnRNPM* transcript, in the form of crRNA from IDT, together with tracrRNA. We assembled the tracrRNA:crRNA duplex by combining 24pmol of tracRNA and 24pmol of crRNA in a volume of 5µl, and incubating at 95°C for 5 min,

followed by incubation at room temperature. 12pmol of recombinant Cas9 (Protein Expression and Purification Facility, EMBL, Heidelberg) were mixed with 12pmol of the tracrRNA:crRNA duplex in OPTIMEM I (GIBCO) for 5min at room temperature and this RNP was used to transfect MKN45 cells in the presence of Lipofectamine RNAiMax. Cells were harvested 48 h later and individual clones were isolated and assayed for hnRNPM downregulation as described above for IQGAP1. The primers used were: Forward: 5'- CACGTGGGCGCGCAGG -3'; Reverse: 5'-GCAAAGGACCGTGGGATACTCAC -3.

Splicing assay

Splicing assays with the DUP51M1 mini-gene reporters were performed as previously described (Damianov et al., 2016). Briefly, cells were co-transfected with DUP51M1 or DUP51-ΔM site plasmids and pCMS-EGFP at 1:3 ratio, for 40 h. Total RNA was extracted using TRIzol Reagent® (Thermo Fisher Scientific) and cDNA was synthesized in the presence of a DUP51-specific primer (DUP51-RT, 5'-AACAGCATCAGGAGTGGACAGATCCC-3'). Analysis of alternative spliced transcripts was carried out with PCR (15-25 cycles) using primers DUP51S_F (5'-GACACCATCCAAGGTGCAC-3') and DUP51S_R (5'-CTCAAAGAACCTCTGGGTCCAAG-3'), followed by electrophoresis on 8% acrylamide-urea gel. Quantification of percentage of exon 2 inclusion was performed with ImageJ or with ImageLab software (version 5.2, Bio-Rad Laboratories) when ^{32}P-labelled DUP51S_F primer was used for the PCR. For the detection of the RNA transcript bound on hnRNPM after UV crosslinking, PCR was performed using primers DUP51UNS_F (5'-TTGGGTTTCTGATAGGCACTG-3') and DUP51S_R (see above).

For the validation of the AS events identified by RNA-seq, cDNA was synthesized from total RNA of appropriate cells in the presence of random hexamer primers and used as a template in PCR with the primers listed in **Table S4**. % inclusion for each event in 3 or more biological replicates was analysed in 8% acrylamide-urea gel and quantified by ImageJ.

UV-crosslinking experiments were performed as described (Damianov et al., 2016). Briefly, monolayer MKN45 cell cultures after transfection with the minigene reporters, as described above, were irradiated with UV (254 nm) at 75 mJ/cm^2 on ice in a UV irradiation system BLX 254 (Vilber Lourmat). UV-irradiated cells were lysed for 5 min on ice with ten packed cell volumes of buffer [20 mM HEPES-KOH pH 7.5, 150 mM NaCl, 0.5 mM DTT, 1 mM EDTA, 0.6% Triton X-100, 0.1% SDS, and 50mg/ml yeast tRNA] and centrifuged at 20,000 x g for 5 min at 4^{0}C. The supernatants were 5 x diluted with buffer [20 mM HEPES-KOH pH 7.5, 150 mM NaCl, 0.5 mM DTT, 1 mM EDTA, 1.25x Complete protease inhibitors (Roche), and 50 μg/ml yeast tRNA]. Lysates were centrifuged for 10 min at 20,000 x g, 4^{0}C prior to IP.

MTT cell proliferation assay

In 96-well plates, cells were seeded at a density of 2×10^3 cells/well in complete RPMI. After 24 hrs, the medium was replaced with serum-free RPMI supplemented with 0.5mg/ml MTT (3-[4,5-dimethylthiazol-2-yl]-2,5-diphenyl tetrazolium bromide; Sigma-Aldrich) colorimetric staining solution for 2h. After the removal of MTT, the cells were mixed with 200μl DMSO and incubated for 5-10min at RT on a shaking platform. The absorbance was read at 570 nm using the SUNRISE^{TM} Absorbance Reader (Tecan Trading AG).

Colony-Formation assay

In 6-well plates, 200 cells/well were placed and allowed to grow for 7 days at 37°C with 5% CO_2. The formed colonies were fixed with 0.5mL of 100% methanol for 20min at RT. Methanol was then removed and cells were carefully rinsed with H_2O. 0.5ml crystal violet staining solution (0.5% crystal violet in 10% ethanol) was added to each well and cells were left for 5min at RT. The plates were then washed with H_2O until excess dye was removed and were left to dry. The images were captured by Molecular Imager® ChemiDoc™ XRS+ Gel Imaging System (Bio-Rad) and colonies were quantified using ImageJ software.

Wound healing assay

Cells were cultured in 24-well plates at 37°C with 5% CO_2 in a monolayer, until nearly 90% confluent. Scratches were then made with a sterile 200µl pipette tip and fresh medium without FBS was gently added. The migration of cells in the same wound area was visualized at 0, 8, 24, 32 and 48 hrs using Axio Observer A1 (Zeiss) microscope with automated stage.

Cell Cycle Analysis

The cells were seeded in 6-well plates at a density of 3×10^5 cells/well. When cells reached 60-80% confluence, they were harvested by trypsinization into phosphate-buffered saline (PBS). The pellets were fixed in 70% ethanol and stored at -20°C till all time-points were collected. On the day of the FACS analysis, cell pellets were washed in phosphate-citrate buffer and centrifuged for 20min. 250µl of RNase/propidium iodide (PI) solution were then added to each sample (at concentrations of 100µg/ml for RNase and 50µg/ml for PI) and cells were incubated at 37°C for 30min. Finally, the cells were analysed through flow cytometric analysis using FACSCanto™ II (BD-Biosciences).

Immunostaining

For immunofluorescence, cells were seeded on glass coverslips and were left to adhere for 24 hrs. Cells were next fixed for 10 minutes with 4% paraformaldehyde PFA (Alfa Aesar), followed by permeabilization with 0.25% (w/v) Triton X-100. Cells were then incubated for 30 min in 5% BSA/PBS (phosphate buffer saline). The primary antibodies used for immunostaining were: anti-hnRNPM (1:300, clone 1D8, NB200-314SS, Novus), anti-IQGAP1 (1:500, ab86064, Abcam or 1:250 sc-374307, Santa-Cruz). For β-tubulin staining, cells were fixed in -20°C with ice-cold methanol for 3 minutes, blocked in 1% BSA/PBS solution and incubated overnight with the primary antibody (1:250, clone 2-28-33, Sigma-Aldrich). After washing with PBS, cells were incubated with secondary antibodies (anti-rabbit-Alexa Fluor 555 or anti-mouse Alexa Fluor 488, both used at 1:500; Molecular Probes) at room temperature for 1h followed by the staining of nuclei with DAPI for 5 min at RT. For mounting Mowiol mounting medium (Sigma-Aldrich) was used and the images were acquired with Leica DM2000 fluorescence microscope or a LEICA SP8 White Light Laser confocal system and were analysed using the Image J software.

Tissue Microarrays (TMA) slides were purchased from US Biomax, Inc (cat. no. T012a). The slides were deparaffinized in xylene and hydrated in different alcohol concentrations. Heat-induced antigen retrieval in citrate buffer pH 6.0 was used. Blocking, incubation with first and secondary antibodies as well as the nuclei staining and mounting, were performed as mentioned above.

Immunohistochemistry and H&E staining

At the end of the xenograft experiment tumours were dissected from the mice, fixed in formalin and embedded in paraffin. Sections were cut at 5 μm thickness, were de-paraffinized and stained for haematoxylin and eosin. For IHC, after de-paraffinization

serial sections were hydrated, incubated in 3% H_2O_2 solution for 10 minutes, washed and boiled at 95°C for 15 minutes in sodium citrate buffer pH 6.0 for antigen retrieval. Blocking was performed with 5% BSA for 1 hr and sections were then incubated with the following primary antibodies overnight at 4°C diluted in BSA: anti Ki-67 (1:200, clone 14-5698-82, ThermoFisher Scientific), hnRNP-M (1:100, clone 1D8, sc-20002, Santa Cruz), IQGAP1 (1:100, ab86064, Abcam). Sections were subsequently washed and incubated with the appropriate secondary antibody conjugated to HRP, HRP-conjugated goat anti-mouse IgG (1:5000, 1030-05, SouthernBiotech) or HRP-conjugated goat anti-rabbit IgG (1:5000, 4050-05, SouthernBiotech) and the DAB Substrate Kit (SK-4100, Vector Laboratories) was used to visualise the signal. The sections were counterstained with hematoxylin and imaged with a NIKON Eclipse E600 microscope, equipped with a Qcapture camera.

Proximity ligation assay

Cells were grown on coverslips (13 mM diameter, VWR) and fixed for 10 min with 4% PFA (Alfa Aesar), followed by 10 min permeabilization with 0.25% Triton X-100 in PBS and blocking with 5% BSA in PBS for 30 min. Primary antibodies: anti-hnRNPM (1:300, clone 1D8, NB200-314SS, Novus), anti-IQGAP1 (1:500, ab86064, Abcam or 1:500, 22167-1-AP, Proteintech) diluted in blocking buffer were added and incubated overnight at 4˚C. Proximity ligation assays were performed using the Duolink kit (Sigma-Aldrich DUO92102), according to manufacturer's protocol. Images were collected using a Leica SP8 confocal microscope.

RNA isolation and reverse transcription

Total RNA was extracted with the TRIzol® reagent (Thermo Fisher Scientific). DNA was removed with RQ1 RNase-free DNase (Promega, WI) or DNase I (RNase-free,

New England Biolabs, Inc, MA), followed by phenol extraction. Reverse transcription was carried with 0.4-1 μg total RNA in the presence of gene-specific or random hexamer primers, RNaseOUT™ Recombinant Ribonuclease Inhibitor (Thermo Fisher Scientific) and SuperScript® III (Thermo Fisher Scientific) or Protoscript II (New England Biolabs) reverse transcriptase, according to manufacturer's instructions.

Mass spectrometry and Proteomics analysis

Anti-IQGAP1 immunoprecipitation samples were processed in collaboration with the Core Proteomics Facility at EMBL Heidelberg. Proteomics analysis was performed as follows: samples were dissolved in 2x Laemmli sample buffer, and underwent filter-assisted sample preparation (FASP) to produce peptides with proteolytic digestion. These were then tagged using 4 different multiplex TMT isobaric tags (ThermoFisher Scientific, TMTsixplex™ Isobaric Label Reagent Set): one isotopically unique tag for each IP condition, namely IQGAP1 IP cancer (NUGC4) and the respective IgG control. TMT-tagged samples were appropriately pooled and analysed using HPLC-MS/MS. Three biological replicates for each IP condition were processed.

Samples were processed using the ISOBARQuant (Breitwieser et al., 2011), an R-package platform for the analysis of isobarically labelled quantitative proteomics data. Only proteins that were quantified with two unique peptide matches were filtered. After batch-cleaning and normalization of raw signal intensities, fold-change was calculated. Statistical analysis of results was performed using the LIMMA (Smyth, 2004) R-package, making comparisons between each IQGAP1 IP sample and their respective IgG controls. A protein was considered significant if it had a $P < 5\%$ (Benjamini-Hochberg FDR adjustment), and a fold-change of at least 50% between compared conditions. Identified proteins were classified into 3 categories: Hits (FDR

threshold= 0.05, fold change=2), candidates (FDR threshold = 0.25, fold change = 1.5), and no hits (see **Table S1**).

For the differential proteome analysis of MKN45 and MKN45-*IQGAP1*^{KO} cells, whole cell lysates were prepared in RIPA buffer [25 mM Tris-HCl (pH 7.5), 150 mM NaCl, 1% NP-40, 0.5% sodium deoxycholate, 0.1% SDS). Samples underwent filter-assisted sample preparation (FASP) to produce peptides with proteolytic digestion[61] and analysed using HPLC-MS/MS. The full dataset is being prepared to be published elsewhere.

RNA-seq analysis

Total TRIzol-extracted RNA was treated with RQ1-RNase free DNase (Promega). cDNA libraries were prepared in collaboration with Genecore, at EMBL, Heidelberg. Alternative splicing was analyzed by using VAST-TOOLS v2.2.2 (Irimia et al., 2014) and expressed as changes in percent-spliced-in values (ΔPSI). A minimum read coverage of 10 junction reads per sample was required, as described (Irimia et al., 2014). Psi values for single replicates were quantified for all types of alternative events. Events showing splicing change (|ΔPSI|> 15 with minimum range of 5% between control and *IQGAP1*-KO samples were considered IQGAP1-regulated events.

ORF impact prediction

Potential ORF impact of alternative exons was predicted as described (Irimia et al., 2014). Exons were mapped on the coding sequence (CDS) or 5'/3' untranslated regions (UTR) of genes. Events mapping on the CDS were divided in CDS-preserving or CDS-disrupting.

RNA maps

We compared sequence of introns surrounding exons showing more inclusion or skipping in IQGAP1-KO samples with a set of 1,050 not changing alternative exons. To generate the RNA maps, we used the rna_maps function (Gohr and Irimia, 2019), using sliding windows of 15 nucleotides. Searches were restricted to the affected exons, the first and last 500 nucleotides of the upstream and downstream intron and 50 nucleotides into the upstream and downstream exons. Regular expression was used to search for the binding motif of hnRNPM (GTGGTGG|GGTTGGTT|GTGTTGT|TGTTGGAG or GTGGTGG|GGTTGGTT|TGGTGG|GGTGG)[13].

Gene Ontology

Enrichment for GO terms was analyzed using ShinyGO v0.61 with P value cut-off (FDR) set at 0.05.

QUANTIFICATION AND STATISTICAL ANALYSIS

Data were analysed using GraphPad Prism 7 software (GraphPad Software). Student's t test (comparisons between two groups), one-way ANOVA were used as indicated in the legends. $p < 0.05$ was considered statistically significant.

Table S3 (Related to Figure 5 and Figure S5). List of AS events in cell cycle-related genes identified as altered upon *IQGAP1*^{KO} that were selected for validation. Events with IDs indicated in bold have not been previously annotated.

	Gene	Name	Reference	Event ID	Event type	eCLIP target	hnRNPM motif	Validated
1	*ACOT9*	acyl-CoA thioesterase 9	ENSG00000123130	HsaEX0001973	exon(s) skipped	+	+	yes
2	*ANAPC10*	anaphase promoting complex subunit 10	ENSG00000164162	**HsaEX1003622**	exon(s) skipped	+	+	yes
3	*ARHGAP27*	Rho GTPase activating protein 27	ENSG00000159314	HsaEX0057994	exon(s) skipped			yes
4	*CCNF*	cyclin F	ENSG00000162063	HsaEX0013643	exon(s) skipped		+	no
5	*CDC25C*	cell division cycle 25C	ENSG00000158402	HsaEX0014017	exon(s) skipped		+	no
6	*CENPV*	centromere protein V	ENSG00000166582	**HsaALTD1033377-**	alternative splice			yes

				3/4	acceptor			
7	*CROCC*	ciliary rootlet coiled-coil, rootletin	ENSG00000058453	HsaEX0017309	exon(s) skipped		+	yes
8	*FIP1L1*	Factor interacting with PAPOLA and CPSF1	ENSG00000145216	HsaEX0025814	exon(s) skipped	+	+	yes
9	*GUCD1*	Guanylyl cyclase domain containing 1	ENSG00000138867	HsaEX0010598	exon(s) skipped		+	no
10	*HAUS2*	HAUS augmin like complex subunit 2	ENSG00000137814	HsaEX0029277	exon(s) skipped			no
11	*KIF2A*	kinesin family member 2A	ENSG00000068796	HsaALTD0003479-2/2	alternative splice acceptor	+		yes
12	*KLHL42*	kelch like family member 42	ENSG00000087448	HsaEX0034749	exon(s) skipped		+	no

13	*LRP8*	LDL receptor related protein 8	ENSG00000157193	HsaEX0036473	exon(s) skipped		+	no
14	*MRI1*	methylthioribose-1-phosphate isomerase 1	ENSG00000037757	HsaEX0040081	exon(s) skipped		+	yes
15	*PSIP1*	PC4 and SFRS1 interacting protein 1	ENSG00000164985	HsaALTA0006757-2/6	alternative splice acceptor			yes
16	*RAB40C*	RAB40C, member RAS oncogene family	ENSG00000197562	HsaEX0051706	exon(s) skipped	+		no
17	*RBM10*	RNA binding motif protein 10	ENSG00000182872	HsaEX0052607	exon(s) skipped	+		yes
18	*SDCCAG3*	serologically defined colon cancer antigen 3	ENSG00000165689	**HsaEX0056720**	exon(s) skipped		+	yes
19	*TRPM4*	transient receptor potential cation channel subfamily M member 4	ENSG00000130529	HsaEX0067406	exon(s) skipped	+		yes

Table S4 (Related to Figure 5 and Figure S5). List of primers used for the validation of the AS events shown in **Supplementary Table 3**.

Gene	**Name**	**Sequence**	**Length**	**Tm (°C)**	**GC (%)**
ACOT9	ACOT9-F	CAAAGGGCAGCTTACTCCTGG	21	61	57
	ACOT9-R	TGCTCCTACTATCTCCCGCAA	21	60.4	52
ANAPC10	ANAPC10-F	GCAGTTGGAAAGGACTGGAACA	22	59	50
	ANAPC10-R	TGGAGCTCTCTTCTACTGGTGT	22	58	50
ARHGAP27	ARHGAP27-F	TCCCTGTCCCTGCCCCTC	18	62.7	72
	ARHGAP27-R	CGGAGCCGCTTTCCCTTG	18	61.1	67
CCNF	CCNF-F	GTCCACTGTAGGTGTGCCAAG	21	59	57
	CCNF-R	GGCCTTCATTGTAGAGGTAGGC	22	58	55
CDC25C	CDC25C-FB	AGCACCTAATGAAATGTAGCCCA	23	58	43
	CDC25C-R	TGCTTCTTGATCTTTCAGGGAA	22	57.6	41
CENPV	CENPV-F	TGAATAATAAGCACATACGATGGAAT	26	57.1	31
	CENPV-R	GCGAGAAGCTGGAACAATGAA	21	59.1	48
CROCC	CROCC-F	CGGGACAAGAACCTGCATCTG	21	61.3	57
	CROCC-R	GAGGGCTACACGGTCCTTCTC	21	61.9	62
FIP1L1	FIP1L1-F	GTACAGCAGGGAAGAACTGGA	21	59.4	52

	FIP1L1-R	GTATGTTGCTGTTCTCATTTGCCC	24	60.9	46
GUCD1	GUCD1-F	ACAGAAGAGACCCGGGTGAAT	21	60.8	52
	GUCD1-R	TTCCTGGGACTCTGCCAGATG	21	61.5	57
HAUS2	HAUS2-F	ACCTGGAAATTGAACTCCTGAAACT	25	60.6	40
	HAUS2-R	TCCTGGCACATGGGTTTCAAC	21	61.1	52
KIF2A	KIF2A-F	CGGCCCAGTCAATTTCCTGAA	21	59	52
	KIF2A-R	TTTCTCTAAGTTCTTGCTGTTGC	23	55	39
KLHL42	KLHL42-F	GTTACAACCCCGAGCAGGATG	21	61	57
	KLHL42-R	CCCCCACGATGTAGATGGTCT	21	61	57
LRP8	LRP8-F	TGATAGCCCTCCTGTGCATGA	21	61	52
	LRP8-R	AATTCCATGAGGCACGAAGGG	21	60.7	52
MRI1	MRI1-F	GACAAGCTGAGCTTCCTCGTC	21	61	57
	MRI1-R	CGGGGATCTGCTCATAGACCA	21	61	57
PSIP1	PSIP1-F	AGAGAAAAGGTGGGAGGAACTT	22	58.9	45
	PSIP1-R	TGTTAATCATAACACAGTAATGCCA	25	57.1	32
RAB40C	RAB40C-F	CTGCTCAAGTTCCTGCTGGTG	21	60.5	57
	RAB40C-R	CCAGCGGTTGGTGATGTCATA	21	61.4	52
RBM10	RBM10-F	GTGGTGACAGGACTGGCCG	19	62.9	68
	RBM10-R	GAAGATTTGTTCCGCATCAGCC	22	60.5	50
SDCCAG3	SDCCAG3-F	CGGGCTAGGCAGGTCGTG	18	62.5	72

	SDCCAG3-R	TTGCATAAATTCTGCTGGCCG	21	59.9	48
TRPM4	TRPM4-F	GGGTCTGAGGAATTCGAGACC	21	59.8	57
	TRPM4-R	TTTAGGGCTGGGGCTTTGGT	20	61.8	55

References

Alfieri, C., Zhang, S., Barford, D. (2017). Visualizing the complex functions and mechanisms of the anaphase promoting complex/cyclosome (APC/C). Open Biol. 7. https://doi.org/10.1098/rsob.170204

Biamonti, G., Caceres, J.F. (2009). Cellular stress and RNA splicing. Trends Biochem. Sci. 34, 146–153. https://doi.org/10.1016/j.tibs.2008.11.004

Bradford, M.M. (1976). A rapid and sensitive method for the quantitation of microgram quantities of protein utilizing the principle of protein-dye binding. Anal. Biochem. 72, 248–254. https://doi.org/10.1006/abio.1976.9999

Breitwieser, F.P., Müller, A., Dayon, L., Köcher, T., Hainard, A., Pichler, P., Schmidt-Erfurth, U., Superti-Furga, G., Sanchez, J.-C., Mechtler, K., Bennett, K.L., Colinge, J. (2011). General statistical modeling of data from protein relative expression isobaric tags. J. Proteome Res. 10, 2758–2766. https://doi.org/10.1021/pr1012784

Cerami, E., Gao, J., Dogrusoz, U., Gross, B.E., Sumer, S.O., Aksoy, B.A., Jacobsen, A., Byrne, C.J., Heuer, M.L., Larsson, E. (2012). The cBio cancer genomics portal: an open platform for exploring multidimensional cancer genomics data. Cancer Discov. 2, 401–404. https://doi.org/10.1158/2159-8290.CD-12-0095

Chiang, T.-W.W., le Sage, C., Larrieu, D., Demir, M., Jackson, S.P. (2016). CRISPR-Cas9D10A nickase-based genotypic and phenotypic screening to enhance genome editing. Sci. Rep. 6. https://doi.org/10.1038/srep24356

Choi, Y.D., Dreyfuss, G. (1984). Isolation of the heterogeneous nuclear RNA-ribonucleoprotein complex (hnRNP): a unique supramolecular assembly. Proc. Natl. Acad. Sci. U. S. A. 81, 7471–7475.

Cvitkovic, I., Jurica, M.S. (2013). Spliceosome database: a tool for tracking components of the spliceosome. Nucleic Acids Res. 41, D132-141. https://doi.org/10.1093/nar/gks999

da Fonseca, P.C.A., Kong, E.H., Zhang, Z., Schreiber, A., Williams, M.A., Morris, E.P., Barford, D. (2011). Structures of APC/C(Cdh1) with substrates identify Cdh1 and Apc10 as the D-box co-receptor. Nature 470, 274–278. https://doi.org/10.1038/nature09625

Damianov, A., Ying, Y., Lin, C.-H., Lee, J.-A., Tran, D., Vashisht, A.A., Bahrami-Samani, E., Xing, Y., Martin, K.C., Wohlschlegel, J.A., Black, D.L. (2016). Rbfox Proteins Regulate Splicing as Part of a Large Multiprotein Complex LASR. Cell 165, 606–619. https://doi.org/10.1016/j.cell.2016.03.040

Datar, K.V., Dreyfuss, G., Swanson, M.S. (1993). The human hnRNP M proteins: identification of a methionine/arginine-rich repeat motif in ribonucleoproteins. Nucleic Acids Res. 21, 439–446.

El Marabti, E., Younis, I. (2018). The Cancer Spliceome: Reprograming of Alternative Splicing in Cancer. Front. Mol. Biosci. 5. https://doi.org/10.3389/fmolb.2018.00080

Engström, Y., Eriksson, S., Jildevik, I., Skog, S., Thelander, L., Tribukait, B. (1985). Cell cycle-dependent expression of mammalian ribonucleotide reductase. Differential regulation of the two subunits. J. Biol. Chem. 260, 9114–9116.

Euhus, D.M., Hudd, C., LaRegina, M.C., Johnson, F.E. (1986). Tumor measurement in the nude mouse. J. Surg. Oncol. 31, 229–234. https://doi.org/10.1002/jso.2930310402

Gao, J., Aksoy, B.A., Dogrusoz, U., Dresdner, G., Gross, B., Sumer, S.O., Sun, Y., Jacobsen, A., Sinha, R., Larsson, E. (2013). Integrative analysis of complex cancer genomics and clinical profiles using the cBioPortal. Sci. Signal. 6, pl1. https://doi.org/10.1126/scisignal.2004088

Gattoni, R., Mahé, D., Mähl, P., Fischer, N., Mattei, M.G., Stévenin, J., Fuchs, J.P. (1996). The human hnRNP-M proteins: structure and relation with early heat shock-induced splicing arrest and chromosome mapping. Nucleic Acids Res. 24, 2535–2542.

Ge, S.X., Jung, D., Yao, R. (2019). ShinyGO: a graphical gene-set enrichment tool for animals and plants. Bioinformatics. https://doi.org/10.1093/bioinformatics/btz931

Gijn, S.E. van, Wierenga, E., Tempel, N. van den, Kok, Y.P., Heijink, A.M., Spierings, D.C.J., Foijer, F., Vugt, M.A.T.M. van, Fehrmann, R.S.N. (2019). TPX2/Aurora kinase A signaling as a potential therapeutic target in genomically unstable cancer cells. Oncogene 38, 852–867. https://doi.org/10.1038/s41388-018-0470-2

Gohr, A., Irimia, M. (2019). Matt: Unix tools for alternative splicing analysis. Bioinforma. Oxf. Engl. 35, 130–132. https://doi.org/10.1093/bioinformatics/bty606

Harvey, S.E., Xu, Y., Lin, X., Gao, X.D., Qiu, Y., Ahn, J., Xiao, X., Cheng, C. (2018). Coregulation of alternative splicing by hnRNPM and ESRP1 during EMT. RNA 24, 1326–1338. https://doi.org/10.1261/rna.066712.118

Hedman, A.C., Smith, J.M., Sacks, D.B. (2015). The biology of IQGAP proteins: beyond the cytoskeleton. EMBO Rep. 16, 427–446. https://doi.org/10.15252/embr.201439834

Heyd, F., Lynch, K.W. (2011). Degrade, move, regroup: signaling control of splicing proteins. Trends Biochem. Sci. 36, 397–404. https://doi.org/10.1016/j.tibs.2011.04.003

Hovhannisyan, R.H., Carstens, R.P. (2007). Heterogeneous ribonucleoprotein m is a splicing regulatory protein that can enhance or silence splicing of alternatively spliced exons. J. Biol. Chem. 282, 36265–36274. https://doi.org/10.1074/jbc.M704188200

Hu, W., Wang, Zhongxia, Zhang, S., Lu, X., Wu, Junyi, Yu, K., Ji, A., Lu, W., Wang, Zhong, Wu, Junhua, Jiang, C. (2019). IQGAP1 promotes pancreatic cancer progression and epithelial-mesenchymal transition (EMT) through Wnt/β-catenin signaling. Sci. Rep. 9, 7539. https://doi.org/10.1038/s41598-019-44048-y

Hu, X., Harvey, S.E., Zheng, R., Lyu, J., Grzeskowiak, C.L., Powell, E., Piwnica-Worms, H., Scott, K.L., Cheng, C. (2020). The RNA-binding protein AKAP8 suppresses tumor metastasis by antagonizing EMT-associated alternative splicing. Nat. Commun. 11, 486. https://doi.org/10.1038/s41467-020-14304-1

Huelga, S.C., Vu, A.Q., Arnold, J.D., Liang, T.Y., Liu, P.P., Yan, B.Y., Donohue, J.P., Shiue, L., Hoon, S., Brenner, S., Ares, M., Yeo, G.W. (2012). Integrative Genome-wide Analysis Reveals Cooperative Regulation of Alternative

Splicing by hnRNP Proteins. Cell Rep. 1, 167–178. https://doi.org/10.1016/j.celrep.2012.02.001

Irimia, M., Weatheritt, R.J., Ellis, J.D., Parikshak, N.N., Gonatopoulos-Pournatzis, T., Babor, M., Quesnel-Vallières, M., Tapial, J., Raj, B., O'Hanlon, D., Barrios-Rodiles, M. (2014). A Highly Conserved Program of Neuronal Microexons Is Misregulated in Autistic Brains. Cell 159, 1511–1523. https://doi.org/10.1016/j.cell.2014.11.035

Jeong, I., Yu, N., Jang, I., Jun, Y., Kim, M.-S., Choi, J., Lee, B., Lee, S. (2018). GEMiCCL: mining genotype and expression data of cancer cell lines with elaborate visualization. Database 2018. https://doi.org/10.1093/database/bay041

Johnson, M., Sharma, M., Brocardo, M.G., Henderson, B.R. (2011). IQGAP1 translocates to the nucleus in early S-phase and contributes to cell cycle progression after DNA replication arrest. Int. J. Biochem. Cell Biol. 43, 65–73. https://doi.org/10.1016/j.biocel.2010.09.014

Kafasla, P., Patrinou-Georgoula, M., Guialis, A. (2000). The 72/74-kDa polypeptides of the 70-110 S large heterogeneous nuclear ribonucleoprotein complex (LH-nRNP) represent a discrete subset of the hnRNP M protein family. Biochem. J. 350 Pt 2, 495–503.

Kafasla, P., Patrinou-Georgoula, M., Lewis, J.D., Guialis, A. (2002). Association of the 72/74-kDa proteins, members of the heterogeneous nuclear ribonucleoprotein M group, with the pre-mRNA at early stages of spliceosome assembly. Biochem. J. 363, 793–799.

Kahles, A., Lehmann, K.-V., Toussaint, N.C., Hüser, M., Stark, S.G., Sachsenberg, T., Stegle, O., Kohlbacher, O., Sander, C., Caesar-Johnson, S.J. et al. (2018).

Comprehensive Analysis of Alternative Splicing Across Tumors from 8,705 Patients. Cancer Cell 34, 211-224.e6. https://doi.org/10.1016/j.ccell.2018.07.001

Levine, M.S., Holland, A.J. (2018). The impact of mitotic errors on cell proliferation and tumorigenesis. Genes Dev. 32, 620–638. https://doi.org/10.1101/gad.314351.118

Li, S., Wang, Q., Chakladar, A., Bronson, R.T., Bernards, A. (2000). Gastric Hyperplasia in Mice Lacking the Putative Cdc42 Effector IQGAP1. Mol. Cell. Biol. 20, 697–701. https://doi.org/10.1128/MCB.20.2.697-701.2000

Lian, A.T., Hains, P.G., Sarcevic, B., Robinson, P.J., Chircop, M. (2015). IQGAP1 is associated with nuclear envelope reformation and completion of abscission. Cell Cycle 14, 2058–2074. https://doi.org/10.1080/15384101.2015.1044168

Llères, D., Denegri, M., Biggiogera, M., Ajuh, P., Lamond, A.I. (2010). Direct interaction between hnRNP-M and CDC5L/PLRG1 proteins affects alternative splice site choice. EMBO Rep. 11, 445–451. https://doi.org/10.1038/embor.2010.64

Mähl, P., Lutz, Y., Puvion, E., Fuchs, J.P. (1989). Rapid effect of heat shock on two heterogeneous nuclear ribonucleoprotein-associated antigens in HeLa cells. J. Cell Biol. 109, 1921–1935. https://doi.org/10.1083/jcb.109.5.1921

McQuin, C., Goodman, A., Chernyshev, V., Kamentsky, L., Cimini, B.A., Karhohs, K.W., Doan, M., Ding, L., Rafelski, S.M., Thirstrup, D. et al. (2018). CellProfiler 3.0: Next-generation image processing for biology. PLOS Biol. 16, e2005970. https://doi.org/10.1371/journal.pbio.2005970

Neumayer, G., Belzil, C., Gruss, O.J., Nguyen, M.D. (2014). TPX2: of spindle assembly, DNA damage response, and cancer. Cell. Mol. Life Sci. CMLS 71, 3027–3047. https://doi.org/10.1007/s00018-014-1582-7

Oltean, S., Bates, D.O. (2013). Hallmarks of alternative splicing in cancer. Oncogene. https://doi.org/10.1038/onc.2013.533

Osman, M.A., Sarkar, F.H., Rodriguez-Boulan, E. (2013). A molecular rheostat at the interface of cancer and diabetes. Biochim. Biophys. Acta 1836, 166–176. https://doi.org/10.1016/j.bbcan.2013.04.005

Pan, Q., Shai, O., Lee, L.J., Frey, B.J., Blencowe, B.J. (2008). Deep surveying of alternative splicing complexity in the human transcriptome by high-throughput sequencing. Nat. Genet. 40, 1413–1415. https://doi.org/10.1038/ng.259

Passacantilli, I., Frisone, P., De Paola, E., Fidaleo, M., Paronetto, M.P. (2017). hnRNPM guides an alternative splicing program in response to inhibition of the PI3K/AKT/mTOR pathway in Ewing sarcoma cells. Nucleic Acids Res. 45, 12270–12284. https://doi.org/10.1093/nar/gkx831

Penas, C., Ramachandran, V., Ayad, N.G. (2011). The APC/C Ubiquitin Ligase: From Cell Biology to Tumorigenesis. Front. Oncol. 1, 60. https://doi.org/10.3389/fonc.2011.00060

Pervouchine, D., Popov, Y., Berry, A., Borsari, B., Frankish, A., Guigó, R. (2019). Integrative transcriptomic analysis suggests new autoregulatory splicing events coupled with nonsense-mediated mRNA decay. Nucleic Acids Res. 47, 5293–5306. https://doi.org/10.1093/nar/gkz193

Ran, F.A., Hsu, P.D., Wright, J., Agarwala, V., Scott, D.A., Zhang, F. (2013). Genome engineering using the CRISPR-Cas9 system. Nat. Protoc. 8, 2281–2308. https://doi.org/10.1038/nprot.2013.143

Rando, O.J., Zhao, K., Crabtree, G.R. (2000). Searching for a function for nuclear actin. Trends Cell Biol. 10, 92–97. https://doi.org/10.1016/S0962-8924(99)01713-4

Ren, J.-G., Li, Z., Crimmins, D.L., Sacks, D.B. (2005). Self-association of IQGAP1: characterization and functional sequelae. J. Biol. Chem. 280, 34548–34557. https://doi.org/10.1074/jbc.M507321200

Sansregret, L., Patterson, J.O., Dewhurst, S., López-García, C., Koch, A., McGranahan, N., Chao, W.C.H., Barry, D.J., Rowan, A., Instrell, R. et al. (2017). APC/C Dysfunction Limits Excessive Cancer Chromosomal Instability. Cancer Discov. 7, 218–233. https://doi.org/10.1158/2159-8290.CD-16-0645

Santos, A., Wernersson, R., Jensen, L.J. (2015). Cyclebase 3.0: a multi-organism database on cell-cycle regulation and phenotypes. Nucleic Acids Res. 43, D1140–D1144. https://doi.org/10.1093/nar/gku1092

Shalgi, R., Hurt, J.A., Lindquist, S., Burge, C.B. (2014). Widespread Inhibition of Posttranscriptional Splicing Shapes the Cellular Transcriptome following Heat Shock. Cell Rep. 7, 1362–1370. https://doi.org/10.1016/j.celrep.2014.04.044

Sherley, J.L., Kelly, T.J. (1988). Regulation of human thymidine kinase during the cell cycle. J. Biol. Chem. 263, 8350–8358.

Shkreta, L., Chabot, B. (2015). The RNA Splicing Response to DNA Damage. Biomolecules 5, 2935–2977. https://doi.org/10.3390/biom5042935

Smith, J.M., Hedman, A.C., Sacks, D.B. (2015). IQGAPs choreograph cellular signaling from the membrane to the nucleus. Trends Cell Biol. 25, 171–184. https://doi.org/10.1016/j.tcb.2014.12.005

Smyth, G.K. (2004). Linear models and empirical bayes methods for assessing differential expression in microarray experiments. Stat. Appl. Genet. Mol. Biol. 3, Article3. https://doi.org/10.2202/1544-6115.1027

Sveen, A., Kilpinen, S., Ruusulehto, A., Lothe, R.A., Skotheim, R.I. (2015). Aberrant RNA splicing in cancer; expression changes and driver mutations of splicing factor genes. Oncogene. https://doi.org/10.1038/onc.2015.318

Van Nostrand, E.L., Pratt, G.A., Shishkin, A.A., Gelboin-Burkhart, C., Fang, M.Y., Sundararaman, B., Blue, S.M., Nguyen, T.B., Surka, C., Elkins, K. et al. (2016). Robust transcriptome-wide discovery of RNA-binding protein binding sites with enhanced CLIP (eCLIP). Nat. Methods 13, 508–514. https://doi.org/10.1038/nmeth.3810

Wang, Z., Burge, C.B. (2008). Splicing regulation: From a parts list of regulatory elements to an integrated splicing code. RNA 14, 802–813. https://doi.org/10.1261/rna.876308

West, K.O., Scott, H.M., Torres-Odio, S., West, A.P., Patrick, K.L., Watson, R.O. (2019). The Splicing Factor hnRNP M Is a Critical Regulator of Innate Immune Gene Expression in Macrophages. Cell Rep. 29, 1594-1609.e5. https://doi.org/10.1016/j.celrep.2019.09.078

White, C.D., Brown, M.D., Sacks, D.B. (2009). IQGAPs in cancer: A family of scaffold proteins underlying tumorigenesis. FEBS Lett. 583, 1817–1824. https://doi.org/10.1016/j.febslet.2009.05.007

Xu, Y., Gao, X.D., Lee, J.-H., Huang, H., Tan, H., Ahn, J., Reinke, L.M., Peter, M.E., Feng, Y., Gius, D. et al. (2014). Cell type-restricted activity of hnRNPM promotes breast cancer metastasis via regulating alternative splicing. Genes Dev. 28, 1191–1203. https://doi.org/10.1101/gad.241968.114

Yamano, H. (2019). APC/C: current understanding and future perspectives. F1000Research 8. https://doi.org/10.12688/f1000research.18582.1

Zhou, Z., He, M., Shah, A.A., Wan, Y. (2016). Insights into APC/C: from cellular function to diseases and therapeutics. Cell Div. 11, 9. https://doi.org/10.1186/s13008-016-0021-6

Zhu, Y., Xu, G., Yang, Y.T., Xu, Z., Chen, X., Shi, B., Xie, D., Lu, Z.J., Wang, P., 2019. POSTAR2: deciphering the post-transcriptional regulatory logics. Nucleic Acids Res. 47, D203–D211. https://doi.org/10.1093/nar/gky830

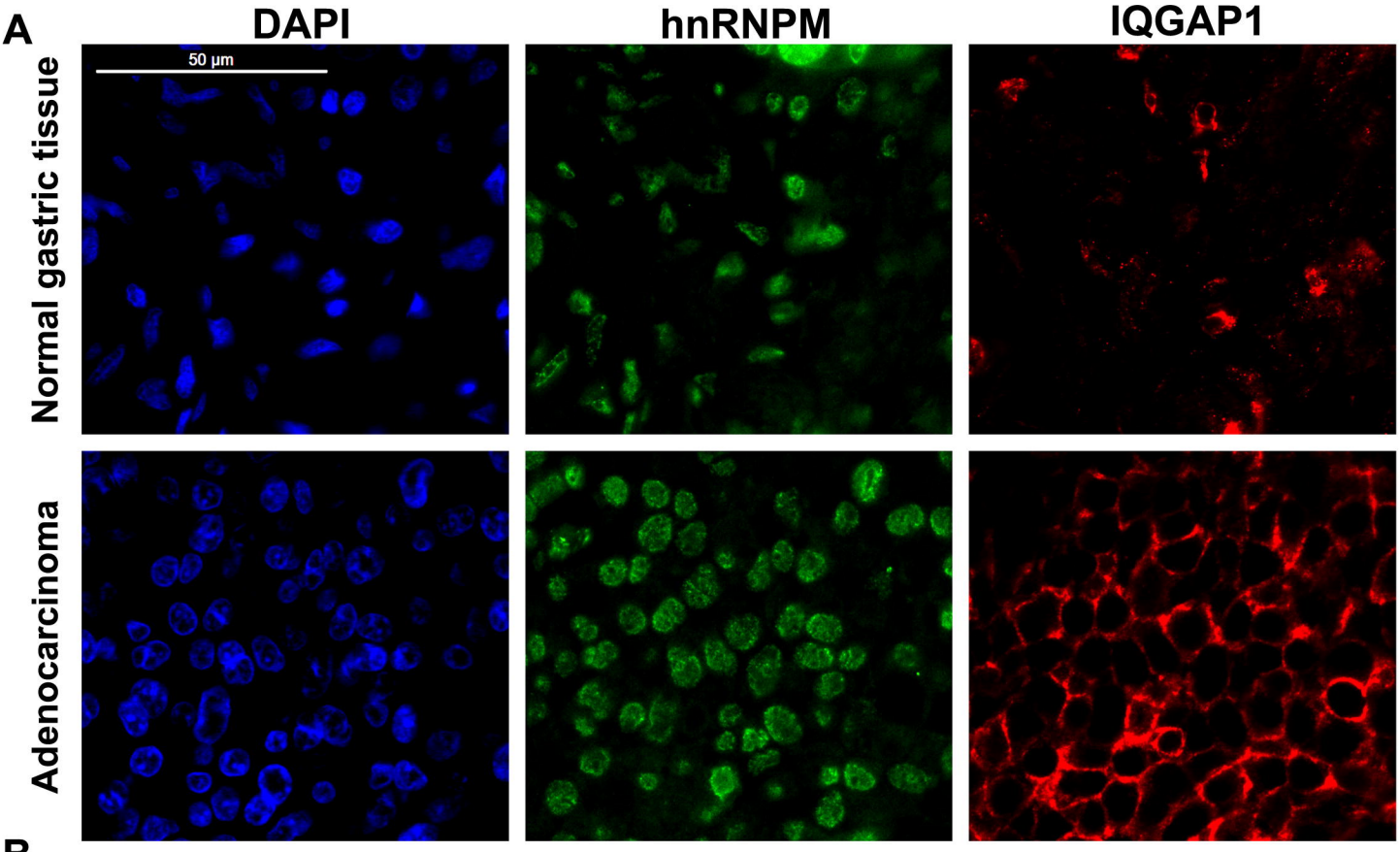
A
DAPI
hnRNPM
IQGAP1
50 μm
Normal gastric tissue
Adenocarcinoma

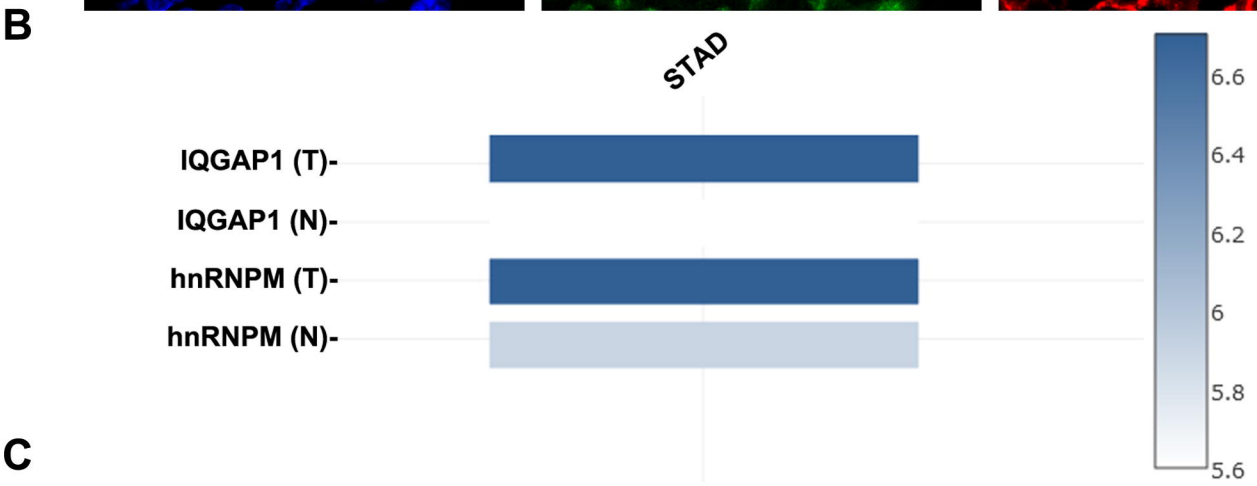
B
STAD
IQGAP1 (T)-
IQGAP1 (N)-
hnRNPM (T)-
hnRNPM (N)-
6.6
6.4
6.2
6
5.8
5.6

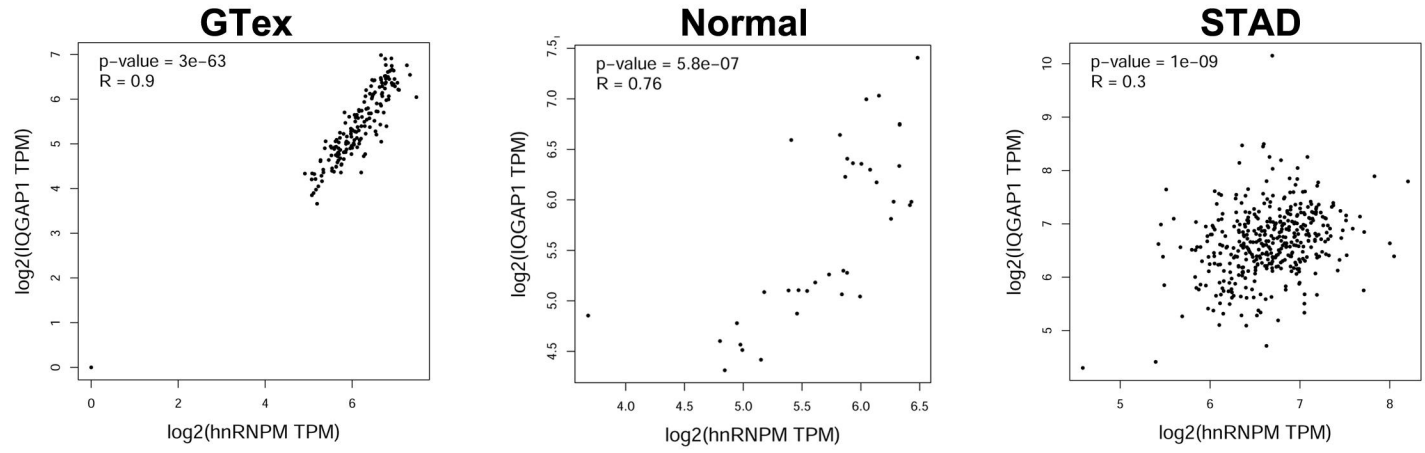
C
GTex
p-value = 3e-63
R = 0.9
log2(IQGAP1 TPM)
log2(hnRNPM TPM)
Normal
p-value = 5.8e-07
R = 0.76
log2(IQGAP1 TPM)
log2(hnRNPM TPM)
STAD
p-value = 1e-09
R = 0.3
log2(IQGAP1 TPM)
log2(hnRNPM TPM)

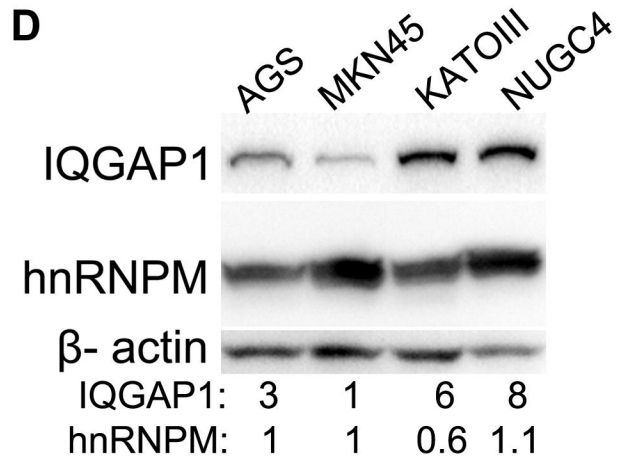
D
AGS
MKN45
KATOIII
NUGC4
IQGAP1
hnRNPM
β- actin
IQGAP1: 3 1 6 8
hnRNPM: 1 1 0.6 1.1

Figure 1

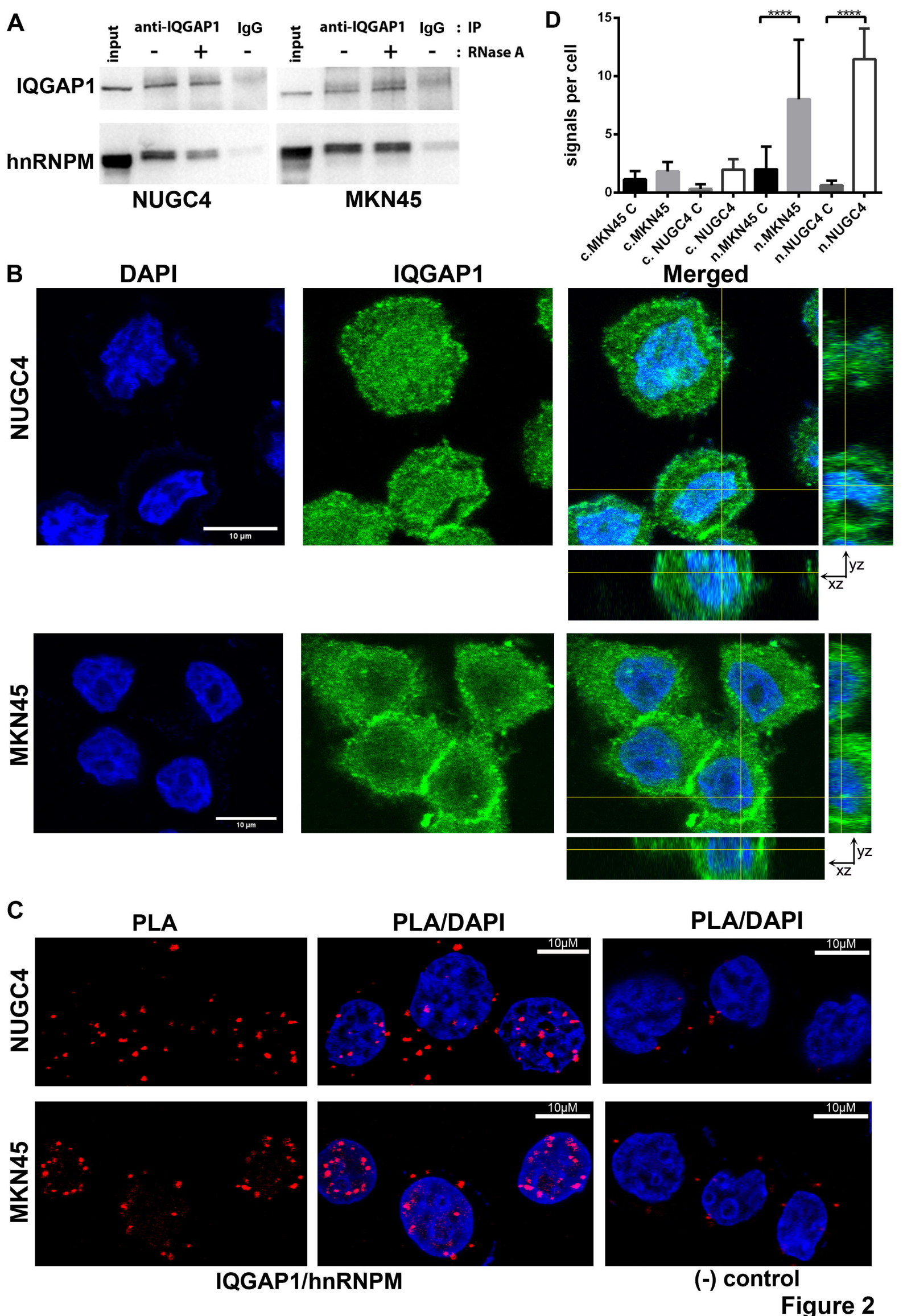
A
input
anti-IQGAP1
IgG
: IP
: RNase A
IQGAP1
hnRNPM
NUGC4
MKN45
D
signals per cell
c.MKN45 C
c.MKN45
c. NUGC4 C
c. NUGC4
n.MKN45 C
n.MKN45
n.NUGC4 C
n.NUGC4
****
B
DAPI
IQGAP1
Merged
NUGC4
MKN45
10 µm
yz
xz
C
PLA
PLA/DAPI
10µM
IQGAP1/hnRNPM
(-) control

Figure 2

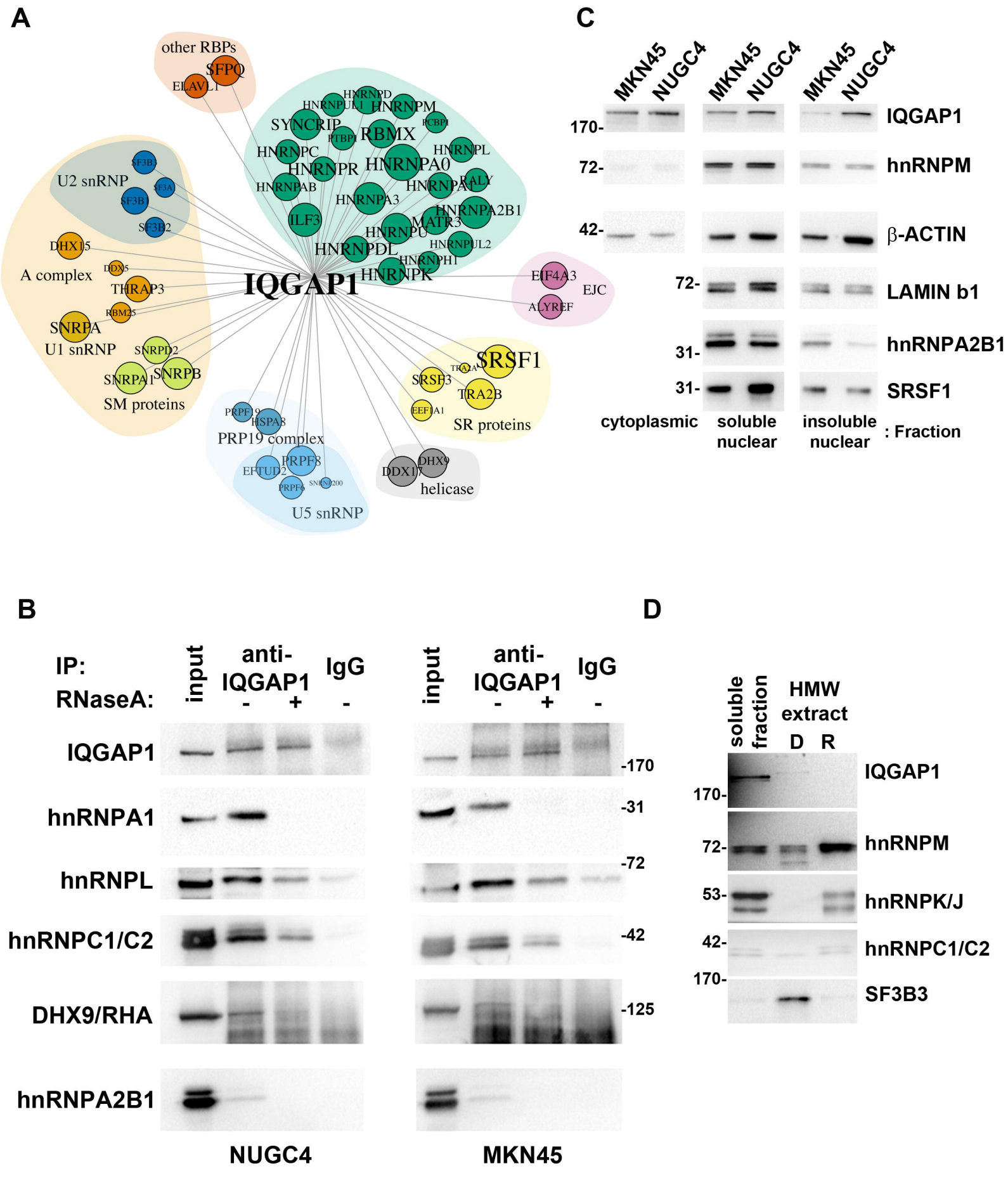
A
other RBPs
SFPQ
ELAVL1
HNRNPD
HNRNPUL1
HNRNPM
SYNCRIP
PCBP1
PTBP1
RBMX
HNRNPC
HNRNPL
HNRNPR
HNRNPA0
HNRNPAB
HNRNPA1
ELAVL1
HNRNPA3
HNRNPA2B1
ILF3
MATR3
HNRNPU
HNRNPUL2
HNRNPDL
HNRNPH1
HNRNPK
U2 snRNP
SF3B4
SF3A1
SF3B1
SF3B2
DHX15
A complex
DDX5
THRAP3
RBM25
IQGAP1
EIF4A3
EJC
ALYREF
SNRPA
U1 snRNP
SNRPD2
SNRPA1
SNRPB
SM proteins
SRSF1
TRA2A
SRSF3
TRA2B
EEF1A1
SR proteins
PRPF19
HSPA8
PRP19 complex
PRPF8
EFTUD2
PRPF6
SNRNP200
U5 snRNP
DHX9
DDX17
helicase
C
MKN45
NUGC4
MKN45
NUGC4
MKN45
NUGC4
170-
IQGAP1
72-
hnRNPM
42-
β-ACTIN
72-
LAMIN b1
31-
hnRNPA2B1
31-
SRSF1
cytoplasmic
soluble nuclear
insoluble nuclear
: Fraction
B
IP:
RNaseA:
input
anti-IQGAP1
IgG
-
+
-
input
anti-IQGAP1
IgG
-
+
-
IQGAP1
hnRNPA1
hnRNPL
hnRNPC1/C2
DHX9/RHA
hnRNPA2B1
-170
-31
-72
-42
-125
NUGC4
MKN45
D
soluble fraction
HMW extract
D
R
170-
IQGAP1
72-
hnRNPM
53-
hnRNPK/J
42-
hnRNPC1/C2
170-
SF3B3

Figure 3

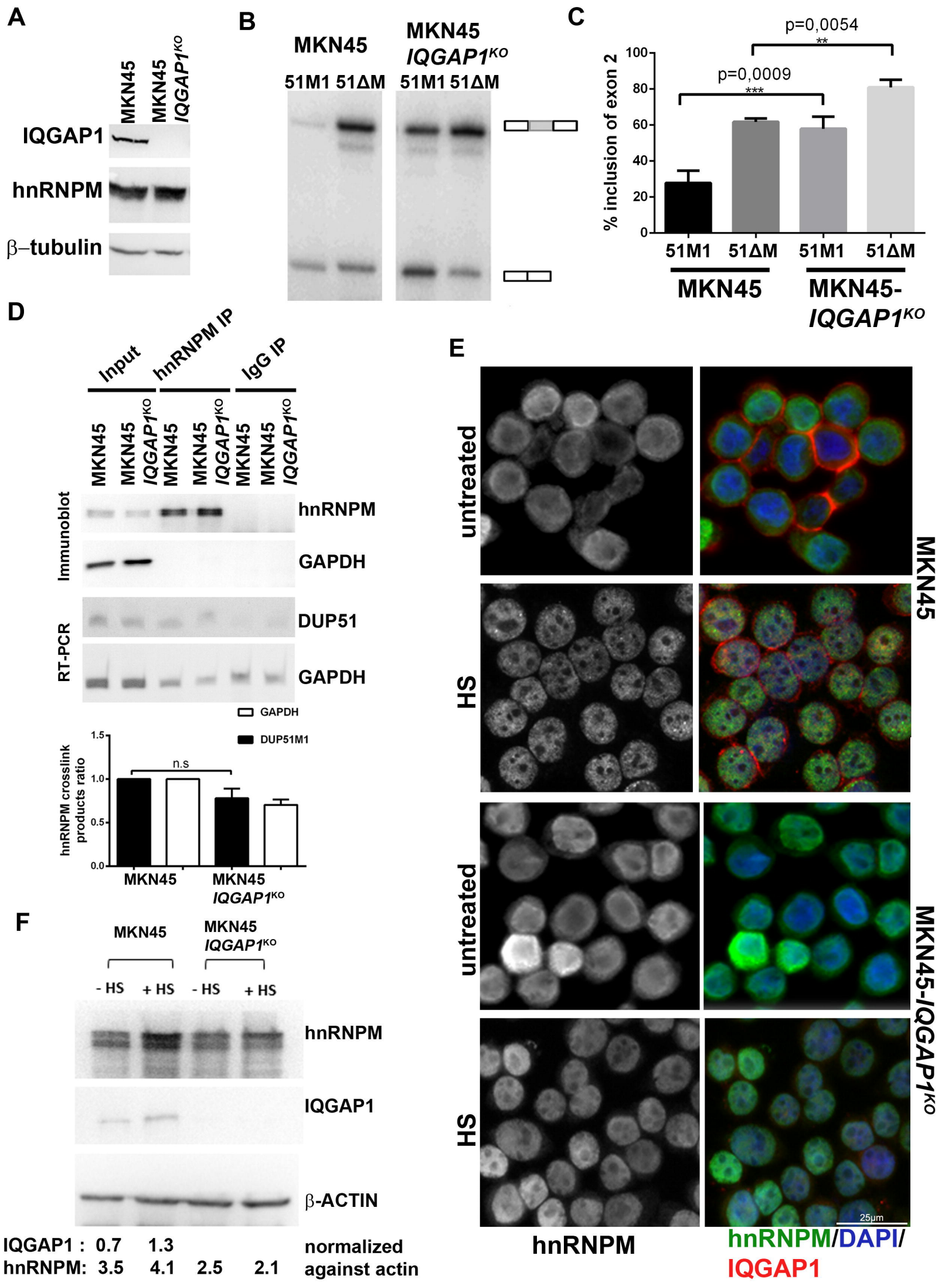
A
MKN45
MKN45 IQGAP1KO
IQGAP1
hnRNPM
β–tubulin
B
MKN45
MKN45 IQGAP1KO
51M1 51ΔM 51M1 51ΔM
C
p=0,0054
**
p=0,0009
***
% inclusion of exon 2
100
80
60
40
20
0
51M1 51ΔM 51M1 51ΔM
MKN45
MKN45-IQGAP1KO
D
Input
hnRNPM IP
IgG IP
MKN45
MKN45 IQGAP1KO
MKN45
MKN45 IQGAP1KO
MKN45
MKN45 IQGAP1KO
Immunoblot
hnRNPM
GAPDH
RT-PCR
DUP51
GAPDH
GAPDH
DUP51M1
hnRNPM crosslink products ratio
1.5
1.0
0.5
0.0
n.s
MKN45
MKN45 IQGAP1KO
E
untreated
HS
untreated
HS
MKN45
MKN45-IQGAP1KO
25µm
hnRNPM
hnRNPM/DAPI/ IQGAP1
F
MKN45
MKN45 IQGAP1KO
- HS + HS - HS + HS
hnRNPM
IQGAP1
β-ACTIN
IQGAP1 : 0.7 1.3
hnRNPM: 3.5 4.1 2.5 2.1
normalized against actin

Figure 4

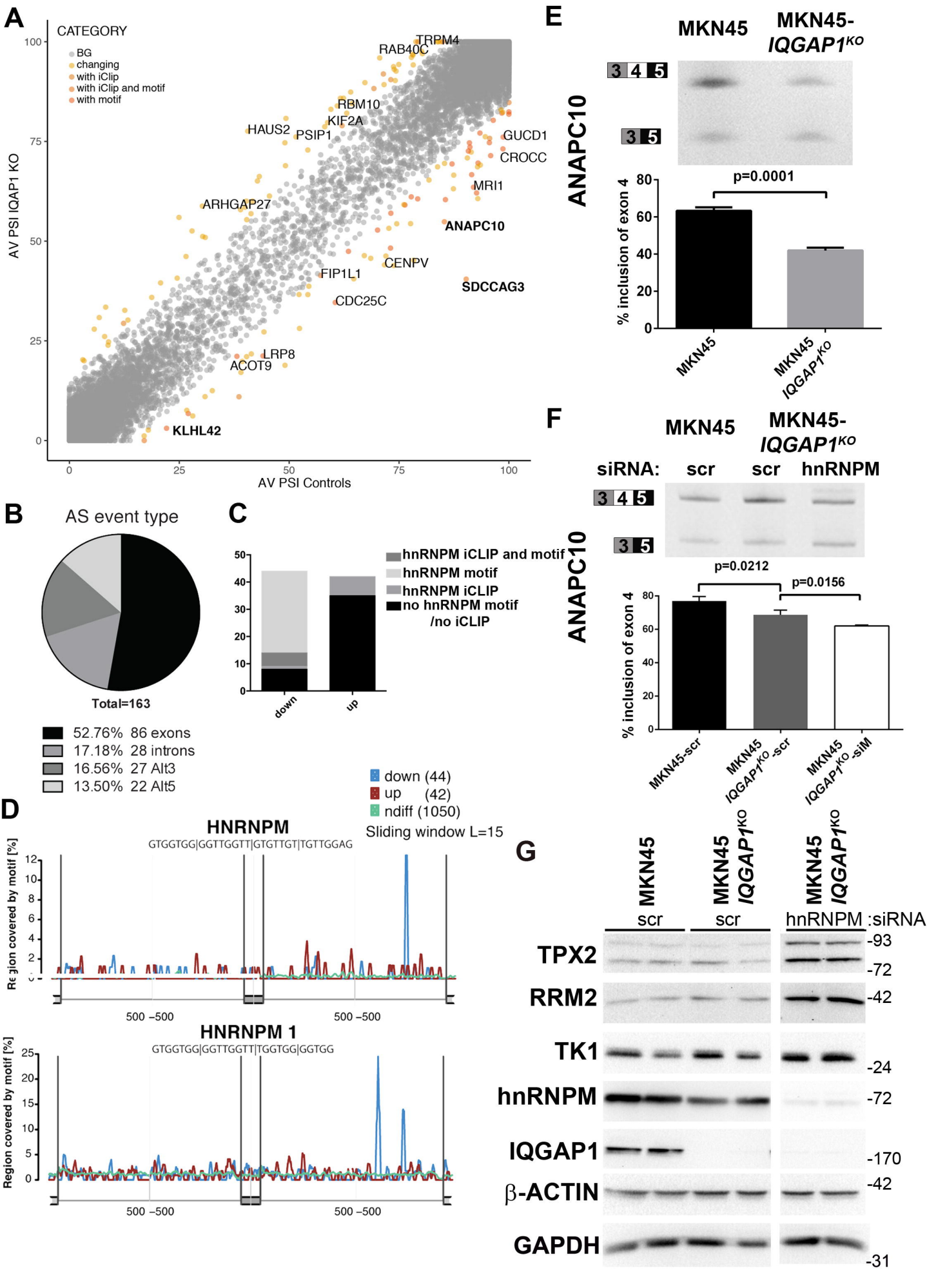
A
CATEGORY
BG
changing
with iClip
with iClip and motif
with motif
AV PSI IQAP1 KO
AV PSI Controls
TRPM4
RAB40C
RBM10
KIF2A
HAUS2
PSIP1
GUCD1
CROCC
MRI1
ARHGAP27
ANAPC10
CENPV
FIP1L1
SDCCAG3
CDC25C
LRP8
ACOT9
KLHL42
B
AS event type
Total=163
52.76% 86 exons
17.18% 28 introns
16.56% 27 Alt3
13.50% 22 Alt5
C
hnRNPM iCLIP and motif
hnRNPM motif
hnRNPM iCLIP
no hnRNPM motif /no iCLIP
down
up
D
down (44)
up (42)
ndiff (1050)
Sliding window L=15
HNRNPM
GTGGTGG|GGTTGGTT|GTGTTGT|TGTTGGAG
Region covered by motif [%]
500 –500
HNRNPM 1
GTGGTGG|GGTTGGTT|TGGTGG|GGTGG
E
MKN45
MKN45-IQGAP1KO
ANAPC10
3 4 5
3 5
p=0.0001
% inclusion of exon 4
MKN45
MKN45 IQGAP1KO
F
MKN45
MKN45-IQGAP1KO
siRNA: scr scr hnRNPM
p=0.0212
p=0.0156
MKN45-scr
MKN45 IQGAP1KO-scr
MKN45 IQGAP1KO-siM
G
MKN45
MKN45 IQGAP1KO
scr scr hnRNPM :siRNA
TPX2
RRM2
TK1
hnRNPM
IQGAP1
β-ACTIN
GAPDH
-93
-72
-42
-24
-72
-170
-42
-31

Figure 5

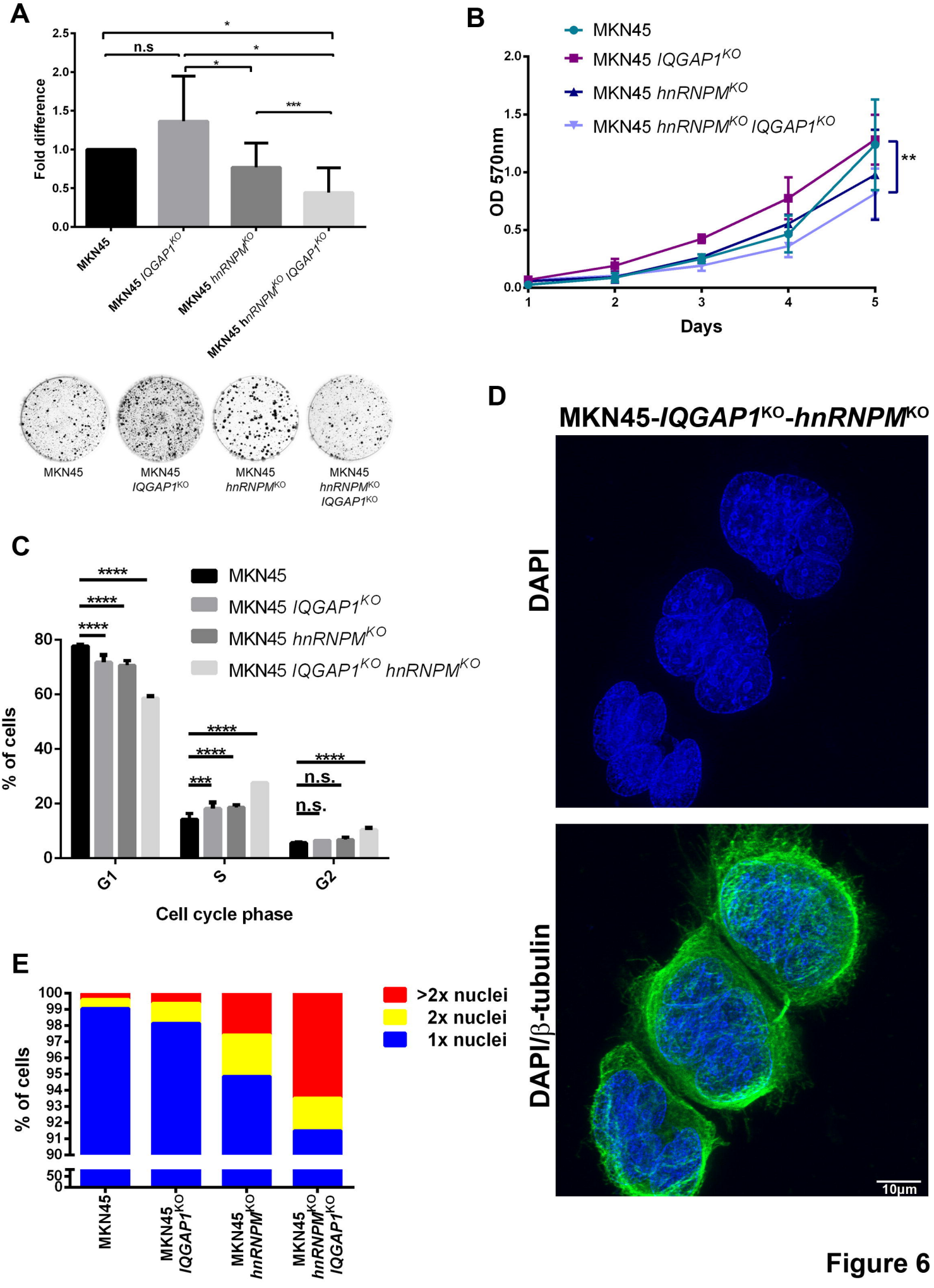
A
Fold difference
n.s
*
*
*
***
MKN45
MKN45 IQGAP1KO
MKN45 hnRNPMKO
MKN45 hnRNPMKO IQGAP1KO
B
MKN45
MKN45 IQGAP1KO
MKN45 hnRNPMKO
MKN45 hnRNPMKO IQGAP1KO
OD 570nm
Days
**
MKN45
MKN45 IQGAP1KO
MKN45 hnRNPMKO
MKN45 hnRNPMKO IQGAP1KO
C
MKN45
MKN45 IQGAP1KO
MKN45 hnRNPMKO
MKN45 IQGAP1KO hnRNPMKO
% of cells
Cell cycle phase
G1
S
G2
****
***
n.s.
D
MKN45-IQGAP1KO-hnRNPMKO
DAPI
DAPI/β-tubulin
10µm
E
% of cells
>2x nuclei
2x nuclei
1x nuclei
MKN45
MKN45 IQGAP1KO
MKN45 hnRNPMKO
MKN45 hnRNPMKO IQGAP1KO

Figure 6

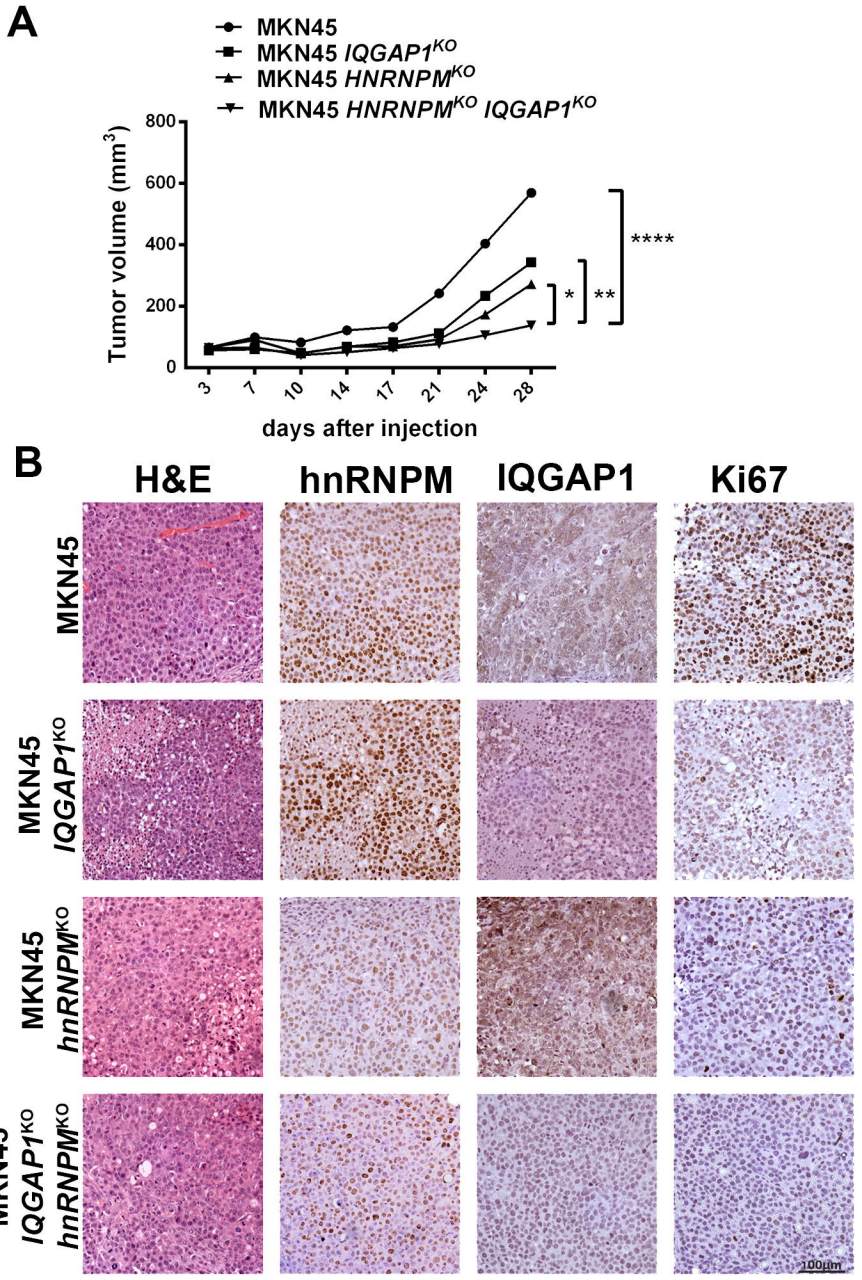
A
MKN45
MKN45 IQGAP1KO
MKN45 HNRNPMKO
MKN45 HNRNPMKO IQGAP1KO
Tumor volume (mm3)
800
600
400
200
0
3
7
10
14
17
21
24
28
days after injection
*
**
****
B
H&E
hnRNPM
IQGAP1
Ki67
MKN45
MKN45 IQGAP1KO
MKN45 hnRNPMKO
MKN45 IQGAP1KO hnRNPMKO
100µm

Figure 7